

## An $SU(2)$ KvBLL caloron gas model and confinement

P. Gerhold, E.-M. Ilgenfritz, and M. Müller-Preussker

*Humboldt-Universität zu Berlin, Institut für Physik,  
Newtonstr. 15, D-12489 Berlin, Germany*

(Dated: July 27, 2006)

A semi-classical model is developed to describe pure  $SU(2)$  Yang-Mills gluodynamics at finite temperature as a dilute, non-interacting gas of Kraan-van Baal-Lee-Lu calorons including the case of non-trivial holonomy. Temperature dependent parameters of the model (asymptotic caloron holonomy, caloron density and caloron size distribution) are discussed from the point of view of lattice observations and of *in-medium* modifications of the one-loop caloron amplitude. Space-like string tensions running into plateaux at distances  $R \approx 0.8 - 1.3$  fm are obtained and compared to lattice results in order to find more precisely the average caloron size. Then, the quark-antiquark free energy as predicted by the model is considered. In the confined phase a linear rise with the separation can be observed up to  $R \approx 4$  fm, whereas it runs into plateaux above  $T_c$ . Screening effects in the adjoint potentials are observed together with an approximate Casimir scaling of the caloron contribution to the fundamental and adjoint forces. In Abelian projection, space-like percolation of monopoles is found in the confined phase only. Thus, taking the non-trivial holonomy into account, confinement properties of pure  $SU(2)$  Yang-Mills gluodynamics can be described by a semi-classical approach up to distances one order of magnitude larger than the caloron size.

PACS numbers:

Keywords:

### I. INTRODUCTION

Lattice QCD provides an *ab initio* description of fundamental features of the hadronic world. It would be useful, however, to have a continuum model of the vacuum structure able to reproduce a variety of lattice results and eventually allowing to compute other quantities not accessible in Euclidean lattice QCD.

What we have in mind here is a reference model that could create an ensemble of non-Abelian gauge fields, not just various Abelian or center projections thereof, analogous to the ansatz by Callan, Dashen and Gross [1], who proposed to describe the QCD vacuum as a superposition of a dilute set of instantons. This approach, widely known as 'dilute gas approximation' (DGA), was refined by many authors. Numerical calculations in such instanton based models have been performed by sampling the collective parameters of their building blocks [2]. In the case of the 'random instanton liquid model' (RILM) [3] the collective parameters were sampled directly (independently), whereas importance sampling was used in the so-called 'interacting instanton liquid model' (IILM) [4, 5] in order to account for the residual interactions between the pseudoparticles, which are induced by temperature and/or the exchange of fermions.

More recently, superpositions of regular gauge instantons, which are strongly interacting due to the slow decay of  $A_\mu(x)$ , have been considered for

which importance sampling is indispensable [6]. In the present paper we wish to extend the RILM in another direction, choosing more general pseudoparticles, calorons with generic holonomy, as the basic building blocks.

Expanding the Euclidean action around such a solution and using the method of collective coordinates [7], it is possible to present the result of quantum fluctuations (gauge fixing terms are suppressed) as an expression like

$$Z_1 = e^{-S_E[A_\mu^{\text{cl}}]} \int dC J(C) (\det' M(C))^{-\frac{1}{2}}, \quad (1)$$

which is the single-pseudoparticle contribution to the partition function. Here  $\det' M(C)$  denotes the non-zero mode determinant of the Hessian  $M(C)$  of the Euclidean action  $S_E[A]$ , parametrized by the collective coordinates (moduli)  $C$  of the classical solution  $A^{\text{cl}}$ . Furthermore, the integrand in (1) includes a Jacobian  $J(C)$ , which contains the metric  $g$  in the moduli space in the form  $\sqrt{\det g}$  built from the zero modes  $\frac{\partial A^{\text{cl}}}{\partial C}$ . As long as interactions are negligible, the integrand in (1) is the probability distribution used for the direct sampling of collective parameters for superpositions of solutions of this type. The actual density of such lumps must be taken as given by (say, lattice) observations. Indeed, a lumpy structure has been observed (and its instanton nature taken for granted) in lattice studies using techniques like cooling or smoothing [8, 9, 10, 11, 12] or smearing [13].

The example of the instanton liquid shows that the contributions *only of small* instantons are well under perturbative control by the instanton transition amplitude calculated by 't Hooft [14]. The behavior in the infrared (*i. e.* the probability of large instantons) is described by other (mainly classical or Higgs-like) interaction effects dealt with in a mean-field fashion [15] or by variational techniques [16]. Irrespective of these less determined details, the model defines what we consider as a model of semi-classical type, in the sense that the building blocks of the model are classical solutions of the Euclidean equations of motion.

Generically, as the result of mixing of the zero modes of individual instantons, the model explains the occurrence of a band of near-zero modes, *i.e.* chiral symmetry breaking [17]. The instanton liquid model is successfully describing hadronic correlators and details of hadronic structure [18, 19, 20] and is one variant of solving the  $U(1)_A$  problem [21]. However, without adding intricate instanton correlations, the instanton liquid model could not describe confinement [22]. This was the motivation to consider strongly correlated instantons in the regular gauge [6]. Our paper is aiming to show that the lack of confinement can be overcome, for temperatures in the confining phase, by the extension of the model from the weakly interacting, singular-gauge instanton (caloron) type of classical solutions to more general solutions with non-trivial holonomy [23, 24, 25, 26].

This extension of the parameter space of the underlying classical solutions can be motivated by both: analytical considerations [27], as discussed in the following Section, as well as by lattice observations [28, 29, 30, 31, 32, 33, 34, 35, 36]. In Refs. [28, 30, 31]  $SU(2)$  lattice gauge fields have been analyzed using smearing techniques and studying their monopole cluster structure. Below the critical temperature a part of the emerging topological clusters could then be characterized to correspond either to non-static calorons or to static dyons in the context of Kraan-van Baal-Lee-Lu caloron solutions with non-trivial holonomy [23, 24, 25, 26]. The relative abundance of topological objects with non-trivial holonomy was furthermore shown to be temperature dependent and to decrease above the critical temperature. In Refs. [33, 34]  $SU(3)$  Monte-Carlo gauge fields have been examined by studying the fermionic zero modes. Configurations with topological charge  $Q = \pm 1$  probably indicating a 3-dyon structure have been identified. The 3-dyon structure is a direct fea-

ture of Kraan-van Baal-Lee-Lu caloron solutions in  $SU(3)$  with non-trivial holonomy, while it can neither be explained as appropriate embeddings of  $SU(2)$  instantons into  $SU(3)$ , nor with calorons with trivial holonomy. A full characterization of  $SU(3)$  caloron solutions by cooling techniques has been given in Ref. [36].

This paper is organized as follows: In Section II we will briefly describe the new type of classical solutions, calorons of generically non-trivial holonomy, to be used in the extension of the instanton liquid model. In Section III we will describe the problems encountered in the construction of superpositions of calorons with non-trivial holonomy. In Section IV we will demonstrate that, under otherwise similar conditions, non-trivial *vs.* trivial holonomy determines whether the caloron gas confines or not. In Section V we will discuss realistic input parameters for the model, in particular the analog of the instanton size distribution, *i. e.* the distribution of the dipole moment of the calorons in terms of their constituent monopoles.

Already here a general remark is in order for the orientation of the reader: all this could be realized in a continuum model. For practical reasons, however, we will discretize the generated gauge field configurations on a suitable grid such that the use of lattice techniques becomes possible. In Section VI the simulation results for the spatial string tensions and the color averaged free energies obtained from our model will be presented, before we proceed to Section VII where we will discuss indirect indicators for confinement observed in the monopole structure of the generated caloron ensembles (via maximal Abelian gauge and Abelian projection). In Section VIII we shall draw conclusions and give an outlook of what should be done next.

## II. CLASSICAL SOLUTIONS OF $SU(2)$ YANG-MILLS THEORY

The instanton, discovered in 1975 [2], is a classical solution of the Euclidean Yang-Mills equation of motion at zero temperature with localized action density, carrying one unit of topological charge. For any number of colors, the instanton is basically an  $SU(2)$  object that is parametrized by  $4 \cdot N_{\text{color}} = 8$  collective coordinates, which are its four-dimensional position in space-time, a size parameter and three parameters describing a global rotation in  $SU(2)$  group space. For higher  $N_{\text{color}}$  the additional parameters describe the embedding of  $SU(2)$  into  $SU(N_{\text{color}})$ . Classical solu-

tions with higher topological charge can in principle be constructed by means of the ADHM formalism [37], although they are not analytically available in general.

The analog of the instanton in the case of non-zero temperature  $T = 1/\beta \neq 0$  was discovered soon after the  $T = 0$  instanton by Harrington and Shepard in 1978 [38] and was accepted as an appropriate semi-classical background at finite temperature. It will be referred to as ‘‘HS caloron’’ throughout the present paper.

Twenty years later, Kraan and van Baal [23, 24] and Lee and Lu [26] extended the parameter space of the HS caloron by an additional parameter, the asymptotic holonomy  $\mathcal{P}_\infty$  which is defined as

$$\mathcal{P}_\infty = e^{2\pi i \vec{\omega} \vec{\tau}} = \lim_{|\vec{x}| \rightarrow \infty} P(\vec{x}), \quad (2)$$

where  $\vec{\tau}$  denotes the vector of Pauli matrices and

$$P(\vec{x}) = \hat{P} \exp \left( i \int_0^\beta A_4(\vec{x}, t) dt \right) \in SU(2), \quad (3)$$

where path ordering is implied by the  $\hat{P}$  symbol. The generalized solution, which we will call KvBLL caloron, is reduced to the HS caloron for trivial asymptotic holonomy, taking values in the center of the gauge group,  $\mathcal{P}_\infty \in Z(2)$ . In the case of general  $N_{\text{color}}$ , this solution can also be constructed. It is not a simple embedding of an  $SU(2)$  solution into the bigger group. The present paper, however, is restricted to the case of  $N_{\text{color}} = 2$ .

Soon after the discovery of the respective solutions, instanton ensembles as well as HS caloron ensembles with trivial holonomy have been used to model the QCD vacuum at  $T=0$  or at finite temperature, respectively. Concerning non-trivial holonomy, the ruling opinion was since the beginning of the 1980’s that such classical solutions cannot play a significant role in the QCD partition function. This was due to an argument given by Gross, Pisarski and Yaffe [39] that gauge fields with non-trivial holonomy are exponentially suppressed by the perturbative free energy [40]. Hence, their potential relevance for quark confinement has not been explored so far. However, one has to keep in mind that the argument does not hold for caloron ensembles with a finite density of calorons in space.

Very recently, Diakonov *et al.* have calculated the holonomy dependence of the free energy of a non-interacting KvBLL caloron gas as a consequence of the caloron quantum weight [27].

For sufficiently high temperatures, trivial holonomy was shown to minimize the free energy and seems therefore dominant in the deconfined phase. However, it becomes unstable below a certain temperature. Thus, one may conjecture that KvBLL calorons with non-trivial holonomy may become the relevant degrees of freedom for lower temperatures. With this new argument in mind and with the KvBLL caloron solution at hand it seems a natural step to study KvBLL caloron gas models.

The KvBLL caloron with arbitrary asymptotic holonomy is a self-dual gauge field, *i.e.*  $F_{\mu\nu} = \tilde{F}_{\mu\nu}$  with  $\tilde{F}_{\mu\nu} = \frac{1}{2} \epsilon_{\mu\nu\alpha\beta} F_{\alpha\beta}$ , solving the Euclidean equation of motion at finite temperature. It was first constructed in the so-called algebraic gauge by means of the ADHM formalism [37] by Kraan and van Baal [23, 24] and by Lee and Lu [26] as a self-dual gauge field in flat  $\mathbb{R}^4$  with the periodicity condition  $A_\mu^{alg}(x + \beta \hat{e}_t) = \mathcal{P}_\infty A_\mu^{alg}(x) \mathcal{P}_\infty^\dagger$ , where  $\hat{e}_t$  denotes the unit vector along the time direction. The resulting vector potential  $A_\mu^{alg}$  defined on  $\mathbb{R}^4$  can then be transformed into a self-dual and time-periodic gauge field  $A_\mu^{per}$  defined on  $S^1 \times \mathbb{R}^3$ , by a gauge transformation  $\Omega(x)$  non-periodic in time

$$\begin{aligned} A_\mu^{per}(\vec{x}, t \bmod \beta) &= \Omega(x) A_\mu^{alg}(\vec{x}, t) \Omega^\dagger(x) \\ &\quad - i \Omega(x) \partial_\mu \Omega^\dagger(x), \end{aligned} \quad (4)$$

with  $x = (\vec{x}, t)$  and

$$\Omega(x) = e^{-2\pi i \vec{\tau} \vec{\omega} t / \beta}. \quad (5)$$

This field is carrying one unit of topological charge and the asymptotic holonomy  $\mathcal{P}_\infty$ . It is the KvBLL caloron in the periodic gauge with arbitrary asymptotic holonomy  $\mathcal{P}_\infty = \exp(2\pi i \vec{\omega} \vec{\tau}) \in SU(2)$ , and one finds that the KvBLL caloron is also described by 8 collective coordinates in addition to its holonomy parameter  $\vec{\omega}$ . However, the physical interpretation of these collective coordinates is different from that of the instanton parameters, as will be discussed in the following.

One can imagine the KvBLL caloron in the algebraic gauge as an infinite chain of equally separated, identical instantons in flat  $\mathbb{R}^4$ , aligned along the time direction with each subsequent instanton rotated by the holonomy  $\mathcal{P}_\infty$  relative to the preceding one - as long as the size  $\rho$  of the instantons is small compared to the inverse temperature  $\beta$ . In that case it is appealing to parametrize the caloron in terms of the collective coordinates of the instanton. For  $\rho \ll \beta$  the corresponding caloron consists of one lump of

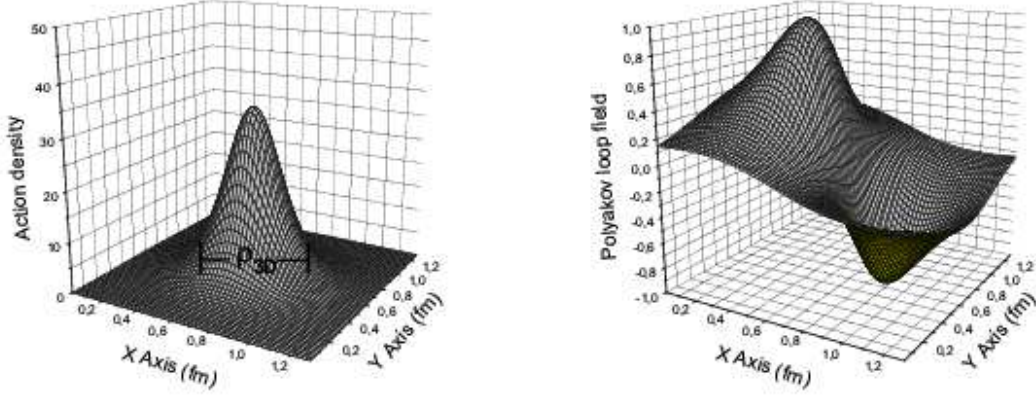


FIG. 1: Action density (left) and Polyakov loop distribution (right) of a KvBLL caloron with maximally non-trivial holonomy  $|\vec{\omega}| = 0.25$ ,  $\rho = 0.33$  fm and  $\beta = 1$  fm, where the action density is given in instanton units  $S_I \times \text{fm}^4$ . Here,  $\rho_{3D}$  denotes the 3D-radius of the almost  $O(4)$ -symmetric caloron action lump.

action, which is approximately  $O(4)$ -rotationally symmetric in space-time, and its radius can be described by the parameter  $\rho$ . Fig. 1 shows the action density and the field of the Polyakov loop  $\ell(x)$ , where

$$\ell(\vec{x}) = \frac{1}{N_{\text{color}}} \text{Tr} P(\vec{x}). \quad (6)$$

This example represents a caloron with maximally non-trivial holonomy and  $\rho \ll \beta$ . The Polyakov loop goes to zero at spatial infinity according to the maximally non-trivial holonomy.

In the opposite case,  $\rho \gg \beta$ , the caloron is dissociated into two constituents, as shown in the action density plot in Fig. 2. For  $\rho \rightarrow \infty$  these constituents become static in time in an appropriate gauge, breaking down the prior  $O(4)$  symmetry to an  $O(3)$ -rotational symmetry in 3-dimensional position space, and the corresponding 3-dimensional radii  $\rho_{3D}^{(1,2)}$  of the two constituents converge to constants approximately given by  $\rho_{3D}^{(1)} \approx \beta/\omega$  and  $\rho_{3D}^{(2)} \approx \beta/\bar{\omega}$ , respectively, where  $\omega = |\vec{\omega}| \in [0; 1/2]$  and  $\bar{\omega} = 1/2 - \omega$ . The constituents can then be identified with BPS monopoles [41] each carrying the fraction  $2\omega$  or  $2\bar{\omega}$ , respectively, of the total action and topological charge. The distance between the monopole positions  $\vec{z}_1, \vec{z}_2$  is given by  $d = |\vec{z}_1 - \vec{z}_2| = \pi\rho^2/\beta$ . Due to the emergence of these two monopoles at larger  $\rho$  it seems more natural to use their positions  $\vec{z}_1$  and  $\vec{z}_2$  for the parametrization of the caloron instead of the instanton parameters involved in the construction scheme. The corresponding vector potentials in the algebraic and

the periodic gauge are then analytically given by [23, 24]

$$A_\mu^{alg}(x) = \frac{\phi}{2} \text{Re} [(\bar{\eta}_{\mu\nu}^1 - i\bar{\eta}_{\mu\nu}^2)(\tau_1 + i\tau_2)\partial_\nu\chi] + \frac{\tau_3}{2} \bar{\eta}_{\mu\nu}^3 \partial_\nu \ln \phi, \quad (7)$$

$$A_\mu^{per}(x) = \frac{\phi}{2} \text{Re} [(\bar{\eta}_{\mu\nu}^1 - i\bar{\eta}_{\mu\nu}^2)(\tau_1 + i\tau_2) \times (\partial_\nu + 4\pi i\omega\delta_{\nu,4})\tilde{\chi}] + \frac{\tau_3}{2} \bar{\eta}_{\mu\nu}^3 \partial_\nu \ln \phi + \delta_{\mu,4} 2\pi\omega\tau_3, \quad (8)$$

with the functions  $\psi(x)$ ,  $\hat{\psi}(x)$ ,  $\phi(x)$ ,  $\chi(x)$ ,  $\tilde{\chi}(x)$  defined according to

$$\psi(x) = \frac{r^2 + s^2 + \pi^2\rho^4}{2rs} \sinh(4\pi r\bar{\omega}) \sinh(4\pi s\omega) + \cosh(4\pi r\bar{\omega}) \cosh(4\pi s\omega) - \cos(2\pi t) + \pi\rho^2 s^{-1} \sinh(4\pi s\omega) \cosh(4\pi r\bar{\omega}) + \pi\rho^2 r^{-1} \sinh(4\pi r\bar{\omega}) \cosh(4\pi s\omega), \quad (9)$$

$$\hat{\psi}(x) = \frac{r^2 + s^2 - \pi^2\rho^4}{2rs} \sinh(4\pi r\bar{\omega}) \sinh(4\pi s\omega) + \cosh(4\pi r\bar{\omega}) \cosh(4\pi s\omega) - \cos(2\pi t), \quad (10)$$

$$\chi(x) = e^{4\pi i t \omega} \frac{\pi\rho^2}{\psi} s^{-1} \sinh(4\pi s\omega) e^{-2\pi i t} + e^{4\pi i t \omega} \frac{\pi\rho^2}{\psi} r^{-1} \sinh(4\pi r\bar{\omega}), \quad (11)$$

$$\tilde{\chi}(x) = e^{-4\pi i t \omega} \chi, \quad (12)$$

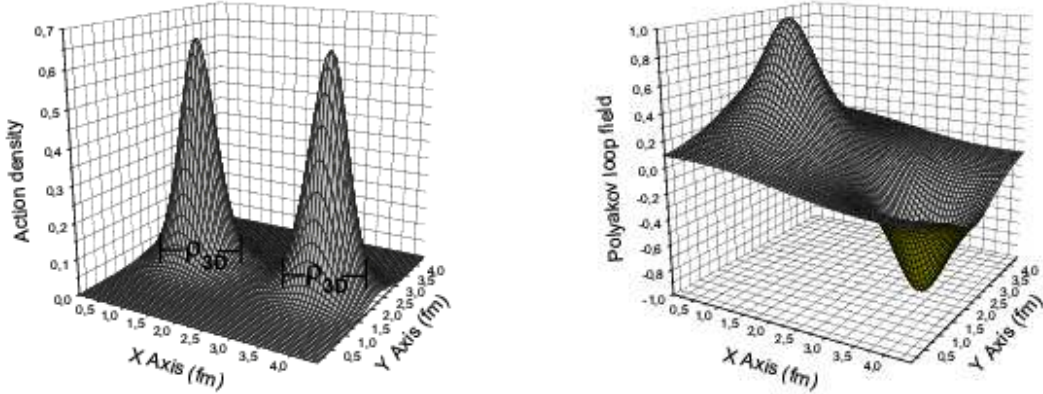


FIG. 2: Action density (left) and Polyakov loop distribution (right) of a dissociated KvBLL caloron with maximally non-trivial holonomy  $|\vec{\omega}| = 0.25$ ,  $\rho = 1$  fm and  $\beta = 1$  fm, where the action density is given in instanton units  $S_I \times \text{fm}^4$ . For growing  $\rho$  two constituents emerge from the spherical action lump shown in Fig. 1. Here,  $\rho_{3D}$  denotes the radius of the almost  $O(3)$ -symmetric monopole action lumps in 3 dimensions.

$$\phi(x) = \frac{\psi}{\bar{\psi}}. \quad (13)$$

Here  $\vec{r} = \vec{x} - \vec{z}_1$ ,  $\vec{s} = \vec{x} - \vec{z}_2$ ,  $r = |\vec{r}|$ ,  $s = |\vec{s}|$ , and  $\bar{\eta}_{\mu\nu}^a$  denotes the 't Hooft symbol [14]. For convenience, the asymptotic holonomy parameter was set equal to  $\vec{\omega}\vec{\tau} = \omega\tau_3$ , the inverse temperature was chosen equal to unity,  $\beta = 1$ , and the constituents were assumed to be separated along the  $z$ -axis, *i.e.*  $\vec{z}_1, \vec{z}_2 \parallel \hat{e}_z$ , with their  $t$ -coordinates set equal to zero. The general gauge field with arbitrary monopole positions, arbitrary temperature and holonomy  $\mathcal{P}_\infty = \exp(2\pi i \vec{\omega}\vec{\tau})$  can be obtained by applying appropriate global transformations on the vector potential. These are a spatial rotation, a translation in space-time, a global gauge rotation  $\Omega$  in color space, accomplishing  $\Omega\omega\tau_3\Omega^\dagger = \vec{\omega}\vec{\tau}$ , and an adequate rescaling. Hence, the KvBLL caloron for a given temperature and fixed holonomy can be parametrized by the four-dimensional position of its center, the size parameter  $\rho$  determining the monopole separation, two angles describing their spatial rotation and one parameter for an residual  $U(1)$  gauge rotation around the axis  $\vec{\omega}\vec{\tau}$  in color space. This is the parametrization that will be applied in the present work. Three further remarks shall be given here.

(i) In the case of non-trivial asymptotic holonomy  $\mathcal{P}_\infty$  the caloron gauge field does not vanish at spatial infinity. In the periodic gauge the  $A_4$  component of the vector potential converges to a constant at spatial infinity whereas the remain-

ing three components go to zero,

$$\lim_{|\vec{x}| \rightarrow \infty} A_4^{per}(x) = 2\pi\vec{\omega}\vec{\tau}, \quad \lim_{|\vec{x}| \rightarrow \infty} A_{1,2,3}^{per}(x) = 0. \quad (14)$$

The non-vanishing vector potential will become an issue when one tries to superpose KvBLL calorons.

(ii) In the case  $\omega \rightarrow 0$  or  $\bar{\omega} \rightarrow 0$  the asymptotic holonomy becomes trivial, one constituent vanishes and the remaining one becomes a HS caloron.

(iii) Finally, the anticaloron, which is the anti-self-dual analogue of the caloron, carrying negative topological charge, can be obtained from the caloron gauge field by

$$\begin{aligned} A_i^{anti}(\vec{x}, t) &= -A_i(-\vec{x}, t), \quad i = 1, 2, 3, \\ A_4^{anti}(\vec{x}, t) &= A_4(-\vec{x}, t). \end{aligned} \quad (15)$$

### III. SUPERPOSITIONS OF CALORONS

There has been remarkable progress in the construction of KvBLL calorons with higher topological charge [42, 43]. Analytical expressions for an arbitrary number of calorons with their monopoles placed along one axis have been derived. Analytical parametrizations for the whole parameter space of classical solutions with arbitrary topological charge, however, are not available in general. Furthermore, configurations of mixed self-dual/anti-self-dual character are not known as solutions of the equations of motion,

just those configurations which are of overwhelming importance. Therefore, the model introduced in this paper will be based on approximate classical gauge field configurations, constructed out of single caloron and anticaloron solutions by some kind of superposition scheme. In the case of the “random instanton liquid” this scheme consisted simply of adding  $N$  single (anti)instanton gauge fields (“sum-ansatz”)

$$A_\mu(x) = \sum_i A_\mu^{(i)}(x), \quad i = 1, \dots, N, \quad (16)$$

where the  $A_\mu^{(i)}(x)$  were chosen in the singular gauge, in which the vector potential outside the instanton core drops to zero most quickly. Due to the non-linearity of  $F_{\mu\nu}$  in terms of the vector potential, this ansatz leads to deviations from exact (anti-)self-duality. However, since the non-linearity arises from the commutator term  $[A_\mu, A_\nu]$ , the superposition approximately describes a classical solution as long as at every space-time position  $x$  the sum of the gauge fields is dominated by the contribution  $A_\mu^{(i)}(x)$  of one single caloron, or if all vector potentials are almost Abelian.

For instantons, the simple sum-ansatz yields good approximations of multi-instanton configurations, unless the separation between the instantons becomes smaller than the size  $\rho$  of their action lumps. The quantitative criterion  $\rho_1^2 \rho_2^2 / |x_1 - x_2|^4 < 1/200$  for the applicability of the sum-ansatz for the superposition of two instantons with sizes  $\rho_1$ , and  $\rho_2$  and positions  $x_1$  and  $x_2$  was established in [15].

When dealing with calorons with non-trivial holonomy this criterion no longer holds because the KvBLL caloron gauge field does not vanish even far away from the monopole locations. At first, the potential  $A_4$  does not vanish at spatial infinity in the case of non-trivial holonomy, inducing a correlation between calorons even at infinite separations. Secondly, there is a string (“Dirac string”) of strong vector potential between the monopoles of a caloron with non-trivial holonomy. Despite its strength, this string is almost free of action, since its vector potential is “fine-tuned”. However, there can be strong interactions between Dirac strings and further calorons. Therefore, more care is required when one is going to apply the simple sum-ansatz to KvBLL calorons with non-trivial holonomy, in order to avoid that the overlapping vector potentials of two calorons spoil the exact (anti-)self-duality of the single solutions.

The first problem can be overcome quite easily by choosing the algebraic gauge for all the

calorons before adding their potentials. In this gauge the potential  $A_4^{alg}$  vanishes at spatial infinity and the sum-ansatz does no longer yield interactions between infinitely far separated calorons. On the other hand, the vector potentials are then no longer periodic. Periodicity has to be restored by applying another gauge transformation to the sum of the vector potentials. This leads to the modified sum-ansatz

$$A_\mu^{per}(x) = e^{-2\pi i t \vec{\omega} \vec{\tau}} \cdot \sum_i A_\mu^{(i),alg}(x) \cdot e^{+2\pi i t \vec{\omega} \vec{\tau}} + 2\pi \vec{\omega} \vec{\tau} \cdot \delta_{\mu,4}. \quad (17)$$

However, this superposition scheme is only valid under the restriction that only calorons and anticalorons with identical holonomy be superposed because the gauge transformation necessary to bring the caloron vector potential from the algebraic to the periodic gauge depends on the holonomy according to (4). It would not be possible to restore the periodicity of a configuration of calorons in the algebraic gauge with a global gauge transformation, if the configuration were consisting of calorons with different holonomies.

The second problem, involving the Dirac strings, will be addressed in an upcoming paper and is not discussed here. Although the construction, helpful in this case, is of principal interest, it will turn out in the following Section that the calorons considered in this model seem to be only weakly dissociated in realistic physical situations. They are mostly merged together into joined action lumps. This implies that interactions between Dirac strings and other calorons hardly occur.

As discussed before for the case of instantons, superposing calorons according to the sum-ansatz (17) becomes unreasonable if the separations between different calorons or their constituents, respectively, become too small. In such cases an improved superposition scheme is needed. A good candidate for such an improved scheme will also be discussed in the upcoming paper. This improved superposition procedure can be derived exploiting the ADHM-formalism and restores Shuryak’s *ratio-ansatz* [44] when applied to instantons. However, for the caloron model, introduced in the current work, it will turn out that the caloron liquid is sufficiently dilute under realistic conditions to *justify* the sum-ansatz. A measure for the quality of a caloron superposition is given by the “action surplus” factor

$$\gamma = \frac{S[\sum A_\mu^{(i)}]}{\sum S[A_\mu^{(i)}]} \quad (18)$$

which becomes unity for exactly (anti-)self-dual configurations, whereas  $\gamma > 1$ , if the classical equation of motion is piecewise violated.

So far, the discussion was referring completely to the continuum. In order to evaluate a certain set of desired observables numerically, it is convenient to introduce a grid (called ‘‘lattice’’ in the following). In the later calculations, the gauge field  $A_\mu(x)$  of the caloron ensemble, which is analytically given by the sum-ansatz, will be represented by a set of link variables according to

$$U_{x,\mu} = \hat{P} \exp \left( i \int_x^{x+a\hat{\mu}} A_\mu(y) dy_\mu \right). \quad (19)$$

The path ordering operator  $\hat{P}$  will approximately be accounted for by dividing each path of integration into  $N$  sub-intervals with their lengths  $a/N \ll \bar{\rho}$  being small compared to the average caloron size, such that the vector potential along these sub-intervals can be assumed to be constant. In the numerical calculations the convergence of the link variables was ensured by adjusting the number of sub-intervals dynamically, corresponding to the variability of the gauge field, and checked by comparing the resulting parallel transporter for different values of  $N$ .

#### IV. CALORON ENSEMBLES WITH TRIVIAL VERSUS NON-TRIVIAL HOLONOMY

Semi-classical studies based on calorons with trivial holonomy, *i.e.* HS calorons, have already extensively been undertaken in the past [39]. Apart from Diakonov’s new argument [27], opening the way to consider calorons with non-trivial holonomy, *i.e.* KvBLL calorons, one may wonder what the most interesting physical objectives are to begin simulations of KvBLL caloron ensembles. A first striking demonstration what the consequences of expanding the caloron parameter space would be, can be given when we compare the heavy quark-antiquark free energy, extracted from the Polyakov-loop correlator in a random ensemble of HS calorons, with the same quantity obtained from random ensembles of KvBLL calorons with maximally non-trivial holonomy.

These ensembles have been created on an open  $32^3 \times 8$  lattice, embedded in a bigger continuum of the same temporal periodicity that is randomly filled with calorons of a certain density. The links have been generated as described

in the previous Section. The inverse temperature has been set equal to  $\beta=1$  fm. Postponing considerations about the realistic choice of the model parameters to Section V we have here assumed a caloron density of  $n=1$  fm<sup>-4</sup> and a caloron size parameter fixed to  $\rho=0.33$  fm. The color-averaged heavy quark-antiquark excess free energy  $F^{avg}(R)$  can be calculated for the generated configurations by means of the Polyakov loop correlator according to

$$F^{avg}(R) = -\frac{1}{\beta} \ln \langle \langle \ell(\vec{x}) \cdot \ell(\vec{y}) \rangle_V \rangle_C, \quad (20)$$

where  $\langle \cdot \rangle_C$  denotes the average over all configurations and  $\langle \cdot \rangle_V$  the volume average over all pairs of lattice sites  $x, y$  with  $R=|\vec{x}-\vec{y}|$  fixed.

Fig. 3a shows  $F^{avg}$  for trivial ( $\omega=0$ ) and maximally non-trivial holonomy ( $\omega=0.25$ ), while all other parameters are kept fixed. The striking observation is that the excess free energy of the pair rises monotonously with the distance  $R$  in the latter case, whereas it runs into a plateau, corresponding to the deconfinement of quarks, for the HS caloron ensemble in the first case. The effect is directly caused by the holonomy. This becomes obvious, if one considers the pair free energy  $F^{avg}$  for asymptotically large distances  $R$ . Then the covariance  $\text{cov}_V(\ell(\vec{x}), \ell(\vec{y}))$  of  $\ell(\vec{x})$  and  $\ell(\vec{y})$ , which is defined as  $\langle [\langle \ell(\vec{x}) \rangle_V - \ell(\vec{x})] \cdot [\langle \ell(\vec{y}) \rangle_V - \ell(\vec{y})] \rangle_V$ , goes to zero and one obtains

$$F^{avg}(R) = -\frac{1}{\beta} \ln \left( \langle \text{cov}_V(\ell(\vec{x}), \ell(\vec{y})) \rangle + \langle \ell \rangle_V^2 \right) \xrightarrow{R \rightarrow \infty} -\frac{1}{\beta} \ln \left( \langle \ell \rangle_V^2 \right). \quad (21)$$

While  $\langle \ell \rangle_V^2 = 0$  for maximally non-trivial holonomy, leading to an infinitely rising quark-antiquark potential, the average Polyakov loop  $\langle \ell \rangle_V^2$  is non-zero for every configuration with  $\omega \neq 0.25$  due to the restriction induced by the superposition scheme, hence forcing the potential to run into a plateau.

The missing *strictly linear* rise of the free energy on the quark separation even for  $\omega = 0.25$ , which would have been expected at large distances  $R$ , is an unsatisfactory feature of this special example with fixed caloron size. It can be ameliorated by sampling the caloron size parameters  $\rho$  according to a distribution  $D(\rho)$  with a finite width. This is demonstrated in Fig. 3b, where a  $\rho$ -distribution  $D(\rho) \propto \rho^{7/3} \exp(-c\rho^2)$  has been used, which will be physically motivated later. Here, the constant  $c$  is determined by fixing the average size parameter  $\bar{\rho}=0.33$  fm. We will return to the question of a realistic  $\rho$ -distribution

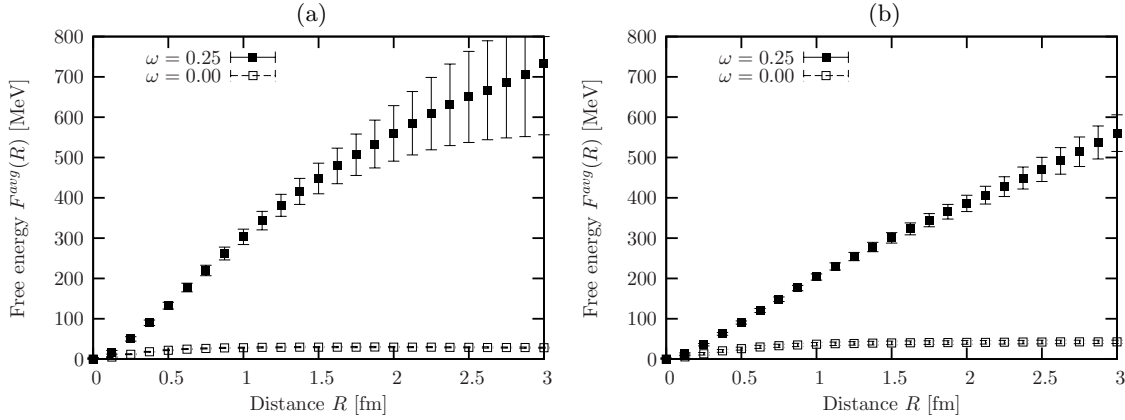


FIG. 3: Heavy quark-antiquark free energy  $F^{avg}(R)$  derived from Polyakov loop correlators measured in caloron ensembles ( $n = 1 \text{ fm}^{-4}$ ,  $\beta = 1 \text{ fm}$ ) with trivial ( $\omega = 0$ ) and maximally non-trivial holonomy ( $\omega = 0.25$ ). (a) The size parameter is fixed to  $\rho = 0.33 \text{ fm}$ . (b) The size parameter is sampled according to a distribution with finite width.

in Section V C. In conclusion of this Section we can state that for caloron gases with temperature, density and caloron size in the right ballpark a reasonable confining potential becomes simply a matter of maximally non-trivial holonomy.

## V. THE PARAMETERS OF THE CALORON GAS MODEL

In the following, for a realistic  $SU(2)$  KvBLL multi-caloron gas model the input parameters will be specified to describe pure gluodynamics. The model is completely defined by describing how the parameters of each single caloron are sampled. The 4-dimensional center position, the spatial orientation of the two monopoles, a global  $U(1)$  rotation around the axis  $\vec{\omega}\vec{\tau}$  in color space will be sampled completely randomly, and the “size” parameter  $\rho$  will be sampled according to a suitable  $\rho$ -distribution  $D(\rho, T)$ . The average number of calorons placed on the lattice is determined by the caloron density  $n(T)$  and the physical four-dimensional volume of the lattice, one extension of which is given by the time periodicity length  $\beta = 1/T$ . Finally, the holonomy parameter  $\vec{\omega}(T)$ , which is assumed to be a function of the temperature, determines the type of superposed solutions. According to the selected superposition scheme introduced in Section III it has to be the same for each superposed caloron in the same configuration. We put  $\vec{\omega}(T) \equiv \omega(T)\hat{e}_3$  without loss of generality. We are aware that this setting breaks the global  $Z(2)$  invariance. It could be easily restored by randomly selecting

values  $\omega(T)$  or  $\bar{\omega}(T) = 0.5 - \omega(T)$ .

Expectation values of observables are then obtained from averaging over the constructed configurations without additional weighing, since the classical action is proportional to the caloron density (apart from local violations of the equation of motion) which is the same for all configurations. Quantum fluctuations are approximately accounted for in the sampling process by an adequate choice of the caloron  $\rho$ -distribution  $D(\rho, T)$ .

The physical scale selected by QCD enters the calculation through the dimensionful parameters of the model, which are the caloron density  $n(T)$  and the  $\rho$ -distribution  $D(\rho, T)$  (both in their dependence on temperature). Finally, in the deconfined phase, the temperature dependence of the holonomy parameter  $\omega(T)$  might be important. These model parameters should be chosen consistently with lattice observations. This will be described in the following and gives the opportunity to discuss what is known about these quantities. We should keep in mind that the confining property is independent of the detailed choice of parameters, as long as maximally non-trivial holonomy is realized in the confined phase.

### A. The holonomy in the confined and deconfined phase

The KvBLL caloron offers the option to set the asymptotic holonomy  $\mathcal{P}_\infty$  to an arbitrary value in  $SU(2)$  through its  $\vec{\omega}$  parameter. In a sufficiently dilute multi-caloron gas the single caloron holonomy parameter  $\vec{\omega}$  determines the volume-



averaged Polyakov loop which is (approximately) selfconsistently determining again the holonomy parameter through  $\langle \ell \rangle_V = \cos(2\pi|\bar{\omega}|)$ . At higher densities this simple relation no longer holds, and the average Polyakov loop is stronger influenced by the internal Polyakov loop profile of the solutions. It becomes a function of the holonomy parameter  $\bar{\omega}$ , the caloron density  $n$ , and the  $\rho$ -distribution. The procedure in the present work is to adopt the holonomy parameter and its dependence on temperature directly from lattice results for the renormalized Polyakov loop.

Obviously, the average Polyakov loop on the lattice is a bare quantity suffering from ultraviolet divergences, since the Polyakov loop is proportional to the propagator of an infinitely massive test quark moving along the time direction. The additive mass shift for the test quark resulting from the lattice regularization affects the expectation value of the Polyakov loop by an exponential factor

$$\langle |\ell| \rangle \propto \exp(-\beta m^{div}) = \exp(-N_\tau a m^{div}) \quad (22)$$

depending on the length of the loop  $\beta$  times a divergent mass  $m^{div}$ , which is proportional to the ultraviolet cutoff

$$m^{div} \propto \frac{1}{a}, \quad (23)$$

where  $a$  is the lattice spacing and  $\beta = N_\tau a$  is the inverse temperature. It has been found numerically in [45] that the divergent mass term  $m^{div}$  is always positive implying that  $\langle |\ell| \rangle$  decreases with finer lattice discretizations  $N_\tau$  along the time direction. For this reason the average *bare* Polyakov loop actually cannot be considered as the caloron holonomy parameter. Since the Polyakov loop is renormalizable [46, 47], it is more appropriate to consider a renormalized Polyakov loop independent of  $N_\tau$ .

A possible renormalization procedure for the Polyakov loop involving its spatial correlation function is presented in Refs. [48, 49], where the renormalized Polyakov loop  $L_{ren}(T)$  was defined through the free energy of a quark-antiquark pair at asymptotic distance. The corresponding results are shown in Fig. 4.

The qualitative statement is that the average Polyakov loop is zero in the confined phase, reflecting the unbroken global  $Z(2)$  symmetry, corresponding to a caloron ensemble with maximally non-trivial holonomy, while it gradually approaches unity above the critical temperature.

Finally, Table I shows for some selected temperatures the renormalized Polyakov loop

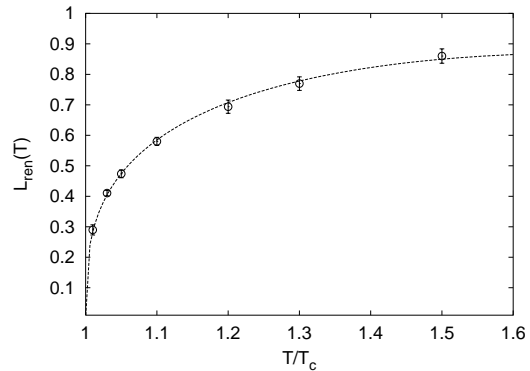


FIG. 4: The renormalized Polyakov loop in  $SU(2)$  LGT versus temperature. The Figure is taken from Digal *et al.* [48].

T	$L_{ren}(T)$	$4\omega(T)$
$\leq T_c$	0.0	1.0
$1.10 T_c$	0.58	0.61
$1.20 T_c$	0.70	0.51
$1.32 T_c$	0.78	0.43
$1.54 T_c$	0.85	0.35
$\gg T_c$	1.0	0.00

TABLE I: Values of the renormalized Polyakov loop as obtained by Digal *et al.* [48]. The holonomy parameter  $\omega(T)$  for the caloron gas model is fixed (up to the  $Z(2)$  symmetry between  $\omega$  and  $\bar{\omega}$ ) by the dilute gas relation  $L_{ren}(T) = \cos(2\pi\omega)$ .

$L_{ren}(T)$  and the corresponding  $\omega$ -parameter in the dilute gas approximation.

## B. Choice of the caloron density

In lattice QCD Monte Carlo studies directly examining the topological structure of the gluonic fields one has attempted to get the instanton (or caloron) density  $n(T)$  by counting the lumps of topological charge. Since such investigations in the past required cooling, instantons (calorons) with sizes close to the lattice spacing have most likely “fallen through the grid”. Furthermore, the sizes of the observed lumps are limited by the lattice size. Therefore, the instanton (caloron) densities obtained through this method are most likely underestimated.

An alternative way to determine the caloron density uses the topological susceptibility  $\chi$  which can be formally defined in Euclidean space-

time by

$$\chi = \int_0^\beta dx_4 \int d^3\vec{x} \langle 0 | \hat{T}(q(x)q(0)) | 0 \rangle, \quad (24)$$

where  $q(x)$  is the operator of the topological charge density and  $\hat{T}$  the time ordering symbol.

A first estimate of  $\chi$  in quenched gauge theory has been obtained from  $1/N_{\text{color}}$  expansion. The Witten-Veneziano formula [50, 51] relates the topological susceptibility of pure gluodynamics to the  $\eta'$  mass elevation from the masses of the pseudoscalar meson octet. This leads to the prediction  $\chi \approx (180 \text{ MeV})^4$ .

The connection to the caloron density  $n$  is established through the functional integration approach, where (24) can be rewritten as

$$\chi = \lim_{V \rightarrow \infty} \frac{\langle Q^2 \rangle}{V}, \quad Q = \int d^4x q(x), \quad (25)$$

if contact terms are omitted. The total topological charge can be related to the numbers  $N^\pm$  of (anti-)calorons in the 4-dimensional volume  $V$  by  $Q = N^+ - N^-$ , assuming that a collection of these objects exhausts the space-time distribution of charge. For an *uncorrelated* caloron gas one would expect a Poisson distribution for  $N^\pm$  with a variance  $\sigma_{N^\pm}^2 = \langle N^\pm \rangle$ , leading to the obvious result

$$n = \chi, \quad (26)$$

where  $n = \langle N^+ + N^- \rangle / V$  is the caloron-plus-anticaloron density.

From the renormalization properties of the Yang-Mills theory, however, it follows that the caloron numbers are *not* Poisson distributed. Instead, the dispersion of  $N^+ + N^-$  is significantly smaller,  $\sigma_{N^+ + N^-}^2 = (4/b) \cdot \langle N^+ + N^- \rangle$ , where  $b = 11N_{\text{color}}/3$ , resulting from some kind of repulsive caloron interaction [16, 52]. Assuming that both species, namely calorons and anticalorons, obey this dispersion relation independently, being still *uncorrelated* among each other, one would get the modified relation [52]

$$n = \frac{b}{4} \chi \quad (27)$$

between density and susceptibility. This would lead to caloron densities approximately twice as high for  $SU(2)$  than in the naive approach. However, despite the existence of caloron interactions, we will adopt an *uncorrelated* sampling of caloron positions since the actual correlation between the

caloron positions remains undetermined. Correspondingly, we will adopt relation (26) for our *uncorrelated* caloron gas model to fix the density  $n(T)$ .

Now the temperature dependence of the topological susceptibility shall be discussed. Several lattice techniques have been applied to estimate  $\chi(T)$ .

The ‘‘cooling method’’ [8, 9] evaluates the susceptibility (25) by measuring the total charge on each independent Monte Carlo configuration by means of an adequate lattice operator  $q_L(x)$ , replacing the continuum operator  $q(x)$ . After some cooling (by local minimization of the action) the (continuum) topological charge  $Q$  of a configuration can be expressed as  $Q_L = \sum_x q_L(x) = Z \cdot Q$  with some renormalization constant  $Z$ . In the confined phase the lattice topological charges  $Q_L$  converge to integer values during the cooling process ( $Z \rightarrow 1$ ), but above the critical temperature these plateaux disappear and the method becomes ambiguous. Therefore, this method is not adequate to monitor the topological susceptibility across the phase transition.

The ‘‘index method’’ [53, 54, 55] determines the topological charge  $Q = n_L - n_R$  via the numbers of righthanded and lefthanded fermionic zero modes. Only Ginsparg-Wilson fermions [56, 57] are sufficiently chiral to allow for an unambiguous definition of chiral modes and, consequently, the topological charge.

The ‘‘field theoretical method’’ applied in [58, 59] evaluates (24) by measuring the correlation function directly on the lattice, without cooling. In this method, the statistical fluctuations could be drastically reduced by using improved operators for the topological charge density obtained from 1 or 2 smearing steps. The lattice susceptibility  $\chi_L$  is connected to the continuum susceptibility  $\chi$  by

$$\chi_L = \langle Q_L^2 / V \rangle = Z^2 a^4 \chi + M \quad (28)$$

with an additional additive renormalization constant  $M$  arising from the contact terms.

In Ref. [58, 59] the susceptibility  $\chi(T)$  for  $SU(2)$  has been obtained by the field theoretical method. Throughout the confined phase, at all  $T < T_c$ , the susceptibility  $\chi(T)$  is equal to the zero-temperature susceptibility  $\chi(T=0)$  (within error bars). Above the critical temperature the topological susceptibility drops to zero. From the 2-smearred results the value  $\chi(T=0) = (198 \pm 8 \text{ MeV})^4$  is obtained. The caloron densities for  $T > T_c$ , that will be adopted for the later calculations, are based on this measurement of  $\chi(T)$  and are presented in Table II.

T	$n(T) = \chi(T)$
$\leq T_c$	$(198 \text{ MeV})^4$
$1.10 T_c$	$(178 \text{ MeV})^4$
$1.20 T_c$	$(174 \text{ MeV})^4$
$1.32 T_c$	$(165 \text{ MeV})^4$
$1.54 T_c$	$(157 \text{ MeV})^4$
$1.79 T_c$	$(136 \text{ MeV})^4$

TABLE II: Approximate dependence of the caloron density  $n(T)$  on the temperature  $T$  according to  $n(T) = \chi(T)$  from (26). The topological susceptibilities  $\chi(T)$  are taken from the  $SU(2)$  results obtained by Alles et al. [58]

At this point it should be stressed once more, that this estimate of  $n(T)$  through  $\chi(T)$  tacitly assumes that there are topological charge-carrying objects (calorons) of charge  $\pm 1$ , and no correlation exists between the placements of single calorons and anticalorons within the volume  $V$ . If there were correlations, the simple estimate of  $n(T)$  would no longer hold. Assuming that calorons are exhausting the topological structure in the deconfined phase, the decline of the topological susceptibility would either imply that the caloron density drops to zero or that topologically uncharged objects like caloron-anticaloron molecules become dominant in the deconfined phase, due to an attractive force between oppositely charged calorons mediated by the exchange of fermions [4, 60].

Since we are dealing with pure Yang-Mills theory, no such correlation will be assumed in the following, and the decreasing topological susceptibility  $\chi(T)$  will be plainly interpreted as a decline of the caloron density  $n(T)$ . However, recent lattice observations [30] have given evidence that calorons and their monopole constituents are not the only type of topological excitations in the deconfined phase. Instead, non-self-dual magnetic objects seem to contribute to the vacuum structure at high temperatures, above  $T_c$ . In this respect the model is certainly not complete to describe the deconfined phase.

### C. Size distributions

At the classical level the action of every single caloron field configuration is  $S_0 = 8\pi^2/g^2$  independent of its collective coordinates and therefore all calorons would contribute equally to the functional integral. However, the classical scale

invariance is broken at the quantum level by the quantum weight as introduced in (1). In the caloron model presented here, the quantum weight will be approximately accounted for by choosing an appropriate size distribution  $D(\rho, T)$  according to the single caloron quantum weight, which is known in 1-loop order. Since the problem has already been encountered in semi-classical simulations based on instantons, let us begin with a short discussion of the instanton size distribution.

#### 1. Instanton size distributions

The calculation of the 1-loop quantum weight in the background of a single instanton in  $SU(2)$  has been performed by 't Hooft [14]

$$Z_1^{\text{inst}} = \int d^4x d^3U d\rho e^{-\frac{8\pi^2}{g^2(\mu)}} f(\rho), \quad (29)$$

$$f(\rho) = \frac{C_0}{4\pi^2} \left( \frac{8\pi^2}{g^2(\mu)} \right)^4 \frac{1}{\rho^5} (\mu\rho)^b,$$

$$b = \frac{11}{3} N_{\text{color}} - \frac{2}{3} N_f, \quad C_0 \approx 0.64191,$$

where the integration  $\int d^4x$  is performed over the four-dimensional instanton position in space-time and  $dU$  denotes the integration over the color group  $SU(2)$  according to the Haar measure. Here,  $\mu$  is the Pauli-Villars mass, *i.e.* the UV cutoff, and  $g^2(\mu)$  denotes the gauge coupling given at this cutoff. Since the quantum weight is proportional to  $\rho^{b-5}$ , it is divergent in the infrared region for  $N_{\text{color}} \geq 2$ . Hence, the integration over the collective instanton coordinates diverges unless the large  $\rho$  tail is suppressed by some other mechanism which would render the model finite.

Several explanations why large instanton sizes could be suppressed in the QCD vacuum (confinement effects, higher order effects, repulsive instanton interactions) are discussed in [61]. Whereas confinement effects were excluded in [61] due to lattice observations, the latter two explanations remain viable mechanisms for the suppression of large instantons. Assuming the running of the coupling constant  $g$  becoming frozen at sufficiently large  $\rho$  due to higher order effects, one obtains a  $1/\rho^5$  tail [62]. Such a behavior was shown to be not in conflict with available lattice data.

A size distribution falling off as  $1/\rho^3$  would directly yield a linear and confining interquark potential with a string tension proportional to the

coefficient in from of the one-over-cube term [63], but this could not be reconciled with lattice data.

A third explanation for the large  $\rho$  suppression takes the statistical mechanics of an interacting instanton gas into account. In [15] the large distance interactions between instantons were treated to be of dipole type as proposed in [1]. Furthermore, a hard-core type repulsion had to be included in order to guarantee the consistency of the calculation. This finally led to an exponential suppression of large instanton sizes, motivating the ansatz for the overall  $\rho$ -distribution

$$D_{inst}(\rho) = a\rho^{b-5}e^{-c\rho^2}. \quad (30)$$

The undetermined constants  $a$  and  $c$  can be fixed by the average instanton size and by normalizing the  $\rho$  distribution. Exponential suppression factors depending on  $\rho^2$  have also been obtained in calculations using variational techniques [16] and in Monte Carlo simulations [64] taking only hard core type interactions [65] into account.

## 2. Caloron size distributions

For KvBLL calorons the calculation of the quantum weight is more difficult and has been performed only recently. Diakonov et al. [27] found an analytical expression for the 1-loop amplitude in the case of an  $SU(2)$  caloron. For the metric in moduli space see also Ref. [66]. In the limit of small  $\rho$  again a factor  $\rho^{b-5}$  emerges. For  $\rho \gg \beta = 1/T$  the quantum weight becomes

$$\begin{aligned} Z_1^{\text{cal}} &= \int d^3z_1 \int d^3z_2 T^6 C \left( \frac{8\pi^2}{g^2} \right)^4 \left( \frac{\Lambda e^{\gamma_E}}{4\pi T} \right)^{\frac{22}{3}} \\ &\times \left( \frac{1}{Tr_{12}} \right)^{\frac{5}{3}} (vr_{12} + 1)^{\frac{4v}{3\pi T} - 1} (\bar{v}r_{12} + 1)^{\frac{4\bar{v}}{3\pi T} - 1} \\ &\times \left( 2\pi + \frac{v\bar{v}}{T} r_{12} \right) e^{-VP(v) - 2\pi r_{12} P''(v) + \dots}, \end{aligned}$$

$$P(v) = \frac{1}{12\pi^2 T} v^2 \bar{v}^2, \quad P'' = \frac{d^2}{dv^2} P(v), \quad (31)$$

where  $C \approx 1.0314$ . Here, the vectors  $\vec{z}_1, \vec{z}_2$  denote the monopole positions,  $r_{12} = |\vec{z}_1 - \vec{z}_2|$  is the monopole separation and  $v = 4\pi\omega T$ ,  $\bar{v} = 4\pi\bar{\omega}T \in [0; 2\pi T]$  determine the caloron holonomy.  $P(v)$  is the 1-loop free energy density for a constant gauge field [40] corresponding to  $v, \bar{v}$ . As expected, this formula reduces to the quantum weight of the HS caloron [39] in the case of trivial holonomy.

For large  $\rho$ , *i.e.* large  $r_{12}$ , the quantum weight is dominated by the exponential expression. The polynomial  $P''(v)$ , appearing in the exponent, is of second order and its zeroes are  $v_{\pm} = \pi T(1 \pm 1/\sqrt{3})$ . Therefore, large  $\rho$  parameters are suppressed by the quantum weight as long as  $v < v_-$  or  $v > v_+$  corresponding to nearly trivial holonomy, whereas in the opposite case the quantum weight diverges exponentially for large  $\rho$ . In the latter case a mechanism to cut off the  $\rho$ -distribution is needed to guarantee that the single caloron remains an important part of the vacuum structure.

For small  $\rho$ , the exponential suppression ansatz (30) reflecting instanton interactions could also be applied to calorons. Since this ansatz has been deduced for instantons interacting like pointlike dipoles, this is a rather crude parametrization for the caloron  $\rho$ -distribution because of its more complex structure with two emerging monopoles. Additionally, the  $\rho$  parameter, which serves as a good approximation for the four dimensional radius of the instanton action lump, does not describe the action lump size in the case of a dissociated caloron. However, for  $\rho \ll \beta$  the caloron is not dissociated and the two monopoles are merged together in one action lump of nearly spherical shape. In this limit  $\rho$  can justifiably be interpreted as caloron size. Then it is reasonable to take over the distribution (30) for sufficiently small calorons, provided that the majority of the calorons is not dissociated.

In a lattice study [67] searching for HS calorons at finite temperatures, the temperature dependent average caloron size  $\bar{\rho}(T)$  has been measured by comparing the topological charge density two-point correlator with that of a superposition of single HS caloron profiles. The conclusion was that in the confined phase the average caloron size as a function of temperature is approximately constant,  $\bar{\rho}(T < T_c) = 0.33$  fm, whereas it falls off in the deconfined phase. Therefore, the same exponential suppression factor  $\exp(-c\rho^2)$  can be applied to calorons at sufficiently small temperatures  $T$  due to  $\bar{\rho}(T)/\beta \ll 1$ .

However, this approximation is only valid up to a certain temperature  $T^* < T_c$  where  $\beta$  becomes of the same order as  $\bar{\rho}$ . Above this temperature  $T^*$  the application of the simple instanton-radius suppression formula to the (already partly dissociated) calorons is no longer justified. Instead, one can consider the statistical mechanics of an interacting monopole gas in a similar manner. Effectively, this can be parametrized by the quantity  $\rho_{3D}$ , which is meant to coincide with  $\rho$  at  $\rho \ll \beta$  (then describing the radius

Temperature	$\rho$ -distribution	fixing of coefficients by
$T < T_c$	$D(\rho, T) = A \cdot \rho^{b-5} \cdot \exp(-c\rho^2)$	$\int D(\rho, T)d\rho = 1, \quad \bar{\rho}$ fixed
$T > T_c$	$D(\rho, T) = A \cdot \rho^{b-5} \cdot \exp(-\frac{4}{3}(\pi\rho T)^2)$	$\int D(\rho, T)d\rho = 1, \quad \bar{\rho}$ running

TABLE III: The  $\rho$ -distributions used in the confined and deconfined phase. In the confined phase the coefficients  $A$  and  $c$  are fixed by reproducing a prescribed average caloron size and the normalization of  $D(\rho, T)$ . In the deconfined phase there is only one coefficient,  $A$ , fixed by normalization.

of the  $O(4)$ -symmetric, non-dissociated caloron), and to provide the 3-dimensional radius of the caloron constituent monopoles (which have identical shape for  $\omega=0.25$ ) at  $\rho \gg \beta$ . Connecting these two limits continuously,  $\rho_{3D}(\rho)$  is a function of the caloron parameter  $\rho$ . In terms of this quantity the statistical mechanics of an interacting monopole gas can effectively be described by the ansatz

$$D_1(\rho, T)d\rho = D_{inst}(\rho_{3D})d\rho_{3D} \quad (32)$$

which should lead to a distribution of the caloron “size” parameter  $\rho$ .

Here, we are using a numerically accessible definition meeting the above requirements. We define  $\rho_{3D}$  as the effective 3-dimensional radius of a region where the action density of a caloron (or of its monopole constituents, respectively) exceeds a certain fraction of the maximal density in the caloron (or monopole) center. Its functional dependence on  $\rho$  is shown in Fig. 5. The precise cut-

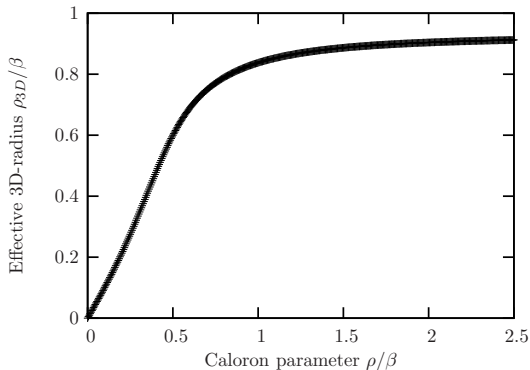


FIG. 5: Dependence of the effective 3-dimensional caloron/monopole radius  $\rho_{3D}$  on the caloron parameter  $\rho$ . Here,  $\rho_{3D}$  is quantitatively defined in the text as the effective, 3-dimensional radius of the region where the action density exceeds a certain fraction of the maximal density in the caloron/monopole center. This fraction is chosen such, that  $\rho_{3D} = \rho$  at  $\rho \ll \beta$ .

off fraction is chosen such that  $\rho_{3D} \approx \rho$  for  $\rho \ll \beta$ . Hence, the ansatz (32) becomes equivalent to the instanton distribution  $D_{inst}(\rho)$  as long as  $\bar{\rho} \ll \beta$ . It also remains applicable at high temperatures.

However, with increasing temperature the extent of the monopoles  $\rho_{3D}$  is kinematically bounded by  $\beta/\omega$ . Therefore, this application of (30) to the interacting monopole gas alone cannot yield a cut off for the  $\rho$ -distribution.

What is needed in order to finally cut-off the  $\rho$ -distribution is a suppression of large distances  $d$  between the constituents. Such an additional suppression factor for large “size” parameters  $\rho \gg \beta$  can be obtained from the quantum weight (31). In [68] the 3-dimensional volume  $V$  in the quantum weight has been interpreted as a specific caloron volume (elementary cell per caloron in a dense packing)  $V_{Cal}(\rho)$  depending on the size parameter  $\rho$ . We introduce a single caloron volume, considered in the limiting case of a well dissociated caloron and dense packing as the volume of a cylinder, circumscribing the caloron

$$V_{Cal}(\rho) = C_0(\omega, T)\pi\beta^2 d, \quad d = \frac{\pi\rho^2}{\beta}. \quad (33)$$

Here  $\beta = 1/T$  sets the scale of the monopole size, and  $d$  is the monopole separation.  $C_0(\omega, T)$  is a holonomy dependent, undetermined factor of order unity. Substituting the volume  $V$  by this ansatz for the specific caloron volume  $V_{Cal}(\rho)$  in the quantum weight (31) and neglecting all non-exponential terms one arrives at the form

$$D_2(\rho, T) \stackrel{\rho \rightarrow \infty}{\sim} e^{-\frac{4}{3}(\pi\rho T)^2 G(\omega)} \quad (34)$$

with

$$G(\omega) = 16C_0(\omega)\pi^2\omega^2\bar{\omega}^2 + 4(\omega^2 + \bar{\omega}^2 - 4\omega\bar{\omega}) \quad (35)$$

for the large  $\rho$  suppression. For trivial holonomy the polynomial  $G(\omega)$  becomes unity, and the well known temperature suppression for the HS calorons [39] is recovered, but for non-trivial holonomy the disastrous repulsive (positive) coefficient of  $d$  appearing in the exponential is now overruled by the specific caloron volume. Choosing  $C_0(\omega, T) > 0.82$  is plausible since  $C_0(\omega, T)$  was assumed to be of order unity. This is sufficient to yield an exponentially suppressed  $\rho$ -distribution even though in this case no caloron interaction (other than the excluded volume interaction) was taken into account. In principle,

the coefficient  $C_0$  has to be determined in a self-consistent way, such that the sum of all specific caloron volumes  $V_{Cal}$  equals the total volume  $V$  up to a factor close to unity.

The strength of this suppression rises with the temperature and depends on the holonomy. Eq. (33), approximating the specific caloron volume as a cylinder, certainly does not hold for the spherical HS calorons well above  $T_c$ . Therefore, this ansatz is assumed to describe the  $\rho$ -distribution at high temperatures but still in the confined phase.

Sewing together both ansatzes corresponding to the opposite temperature regimes  $\bar{\rho} \ll \beta$  and  $\bar{\rho} \gg \beta$  in the simplest form, leads to the ansatz

$$D(\rho, T) = a\rho_{3D}^{b-5} e^{-c\rho_{3D}^2} \cdot \frac{d\rho_{3D}}{d\rho} \cdot e^{-\frac{4}{3}(\pi\rho T)^2 G(\omega)} \quad (36)$$

for the  $\rho$ -distribution in the confined phase. This combination of both approaches guarantees that the average caloron size is bounded from above for all temperatures. To show this, we plot the average caloron size  $\bar{\rho}(T < T_C)$  obtained by this ansatz (36) for the plausible scenario  $\omega = 0.25$ ,  $C_0 = 1$  in Fig. 6 (square symbols). Here  $c$  was determined such that at zero temperature  $\bar{\rho}(T = 0) = 0.33$  fm.

We see, that through this rough ansatz (36) the average of  $\rho$  at any temperature throughout the confined phase,  $\bar{\rho}(T < T_C)$ , is not only bounded but also approximately constant as has been observed in lattice studies [67]. Here it is due to the weakened explicit temperature dependence for  $\omega = 0.25$ .

Since the arguments were rather crude and the coefficient  $C_0$  remains undetermined, only the ubiquitous form of an exponential suppression factor  $\exp(-c\rho^2)$  will be subscribed for our model, while its actual coefficient  $c$  should be fixed according to lattice observations. In principle, these can be obtained by comparing lattice measurements of the topological density correlator with model calculations using the KvBLL caloron profile, analogous to the determination of  $\bar{\rho}(T < T_C)$  performed in [67] which were based on the HS caloron profile. In the following subsection we will find an alternative prescription to fix  $\bar{\rho}(T < T_C)$  based on the space-like string tension leading to a self-consistent tuning for our model.

In the deconfined phase the caloron holonomy ceases to be maximally non-trivial and approaches its trivial value as discussed in Section V A. Therefore, the HS caloron quantum weight, which converges to zero for  $\rho \rightarrow \infty$ , explicitly determines  $D(\rho, T)$  for  $T \gg T_c$ . Since the

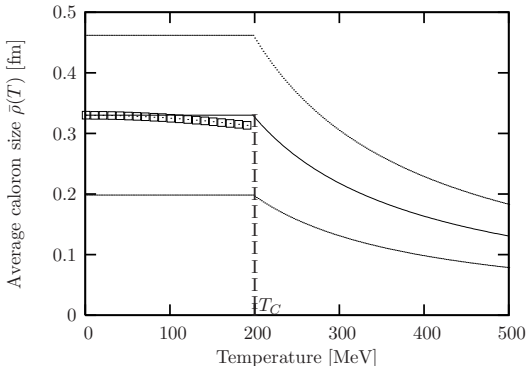


FIG. 6: Illustration of the dependence of the average caloron size  $\bar{\rho}$  (solid) and its interval  $[\bar{\rho} - \Delta_{\bar{\rho}}, \bar{\rho} + \Delta_{\bar{\rho}}]$  of (standard) deviation (dotted) on temperature  $T$ . The two different ansatzes for the  $\rho$ -distributions for the confined/deconfined phase are continuously connected at the critical temperature  $T_c$ . For the curve indicated by open squares see the text.

caloron density  $n(T)$  is assumed to fall off fast beyond the phase transition as argued in Section V B, caloron interactions do not need to be considered. Therefore, the coefficient of  $\rho^2$  in the exponential is exactly known (set by the temperature) and the average caloron size arises directly from (31).

Hence, we are left with two different size distributions for the confined and the deconfined phase, as summarized in Table III. For our model, we sew together these two ansatzes for the  $\rho$ -distribution in a continuous manner, *i.e.*

$$\bar{\rho}(T_C)_{conf.} = \bar{\rho}(T_C)_{deconf.} \quad (37)$$

which is shown in Fig. 6 for the case  $\bar{\rho}(T < T_C) = 0.33$  fm. We will identify the temperature, at which both ansatzes are continuously connected, as the critical temperature  $T_C$ . This establishes a relation between  $\bar{\rho}(T < T_C)$  and  $T_C$  that can be used to fix  $\bar{\rho}(T < T_C)$  in a consistent and unambiguous manner *within* our model.

### 3. Final determination of $\bar{\rho}(T < T_C)$

From lattice calculations [69], the zero-temperature string tension  $\sigma(T=0)$  in terms of the critical temperature is very accurately known for  $SU(2)$  to be  $T_C/\sqrt{\sigma(T=0)} = 0.709$  (4). Furthermore, it is well known that the space-like string tension  $\sigma_S(T)$  coincides with the real (time-like) string tension at  $T=0$ , but stays approximately constant for all temperatures in

the confined phase before it even rises quadratically with  $T$  above the critical temperature [69]. Hence, we obtain the relation for the space-like string tension

$$\sigma_S(T < T_C) \approx \left( \frac{T_C}{0.71} \right)^2. \quad (38)$$

Together with the relation between  $T_C$  and  $\bar{\rho}(T < T_C)$  imposed by (37), one obtains a very precise determination of  $\bar{\rho}(T < T_C)$ , since the space-like string tension  $\sigma_S(T)$  is very sensitive to the average caloron size parameter  $\bar{\rho}(T)$ .

Fig. 7 shows the space-like string tension obtained from our model, as will be described in detail in the next Section, for some selected values of  $\bar{\rho}(T < T_C)$  together with those results for  $\sigma_S(T_C)$ , that are derived from (37) and (38). This approach unambiguously fixes the average caloron size to  $\bar{\rho}(T < T_C) = 0.37$  fm. It should be noticed that this result is not only consistent with the lattice observations for the space-like string tension [69], but also with the direct lattice studies for the caloron size [67], which gave  $\bar{\rho}(T < T_C) = 0.33$  fm. The small deviation of approximately 10% can easily be explained by the fact that the average caloron size in the lattice studies was extracted by assuming the underlying topological objects to be HS-calorons. It would be worthwhile to repeat the calculation of the shape of the topological density correlator for uncorrelated KvBLL calorons and to compare with the data.

As a byproduct of the determination of  $\bar{\rho}(T < T_C)$  we have also fixed the critical temperature  $T_C \approx 178$  MeV as well as the zero-temperature string tension  $\sigma(0) \approx 318$  MeV/fm *within* our model.

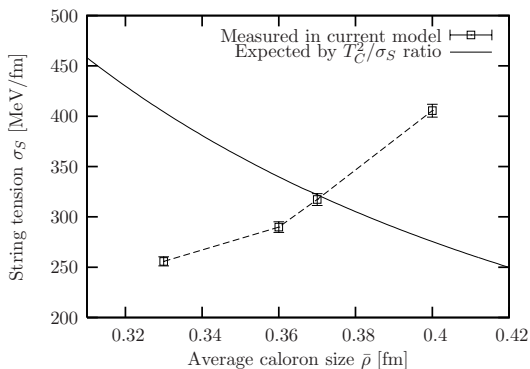


FIG. 7: Space-like string tensions obtained from our model for some selected values of  $\bar{\rho}(T < T_C)$  together with the results for  $\sigma_S(T_C)$  derived from (37) and (38).

## VI. RESULTS FOR INTERQUARK POTENTIALS

Let us now examine the confinement properties of our model at several temperatures. For this purpose, caloron ensembles corresponding to temperatures  $T/T_C = 0.8, 0.9, 1.0$  for the confined and  $T/T_C = 1.10, 1.20, 1.32$  for the deconfined phase have been generated and discretized on suitable lattices. As in Section IV, the lattices do not obey any boundary condition. The performed calculations are *open volume* simulations, since this is the easiest way to guarantee that even strongly dissociated calorons would fit on the lattice. The lattice spacing  $a$  was chosen such, that the ratio  $\bar{\rho}(T)/a$  stays approximately constant for the selected temperatures. The lattice sizes are listed in Table IV together with all other relevant model parameters, which are chosen according to Section V. Table IV also shows the measured *modulus* of the average Polyakov loop  $\langle |\ell| \rangle$  together with the input value of the average Polyakov loop  $\cos(2\pi\omega)$ , as well as the action surplus factor  $\gamma$  as defined in (18). The amount of 60...70% additional action in the confinement phase seems to be acceptable.

We begin with the discussion of the space-like string tension before turning to the more interesting time-like potentials that will be derived from the Polyakov loop correlator. As seen in Section V C 3 the space-like string tension is a sensible tool to determine the caloron size parameter.

### A. Spatial Wilson loops

The color singlet ground state energy of a heavy quark-antiquark pair can be extracted from the Wilson loop

$$W(C_{R,R_T}) = \frac{1}{N_C} \text{Tr} \prod_{l \in C_{R,R_T}} U_l \quad (39)$$

in the limit  $R_T \rightarrow \infty$  according to

$$E(R) = - \lim_{R_T \rightarrow \infty} \frac{1}{R_T} \ln \langle W(C_{R,R_T}) \rangle + C_0, \quad (40)$$

where  $C_{R,R_T}$  denotes a rectangular path with spatial and temporal extent  $R$  and  $R_T$ , respectively. However, at finite temperature this limit can not be realized due to the compactification of time. Instead, *spatial* Wilson loops  $W(C_{R,R_2})$  and their associated potential will be considered here. It is supposed to coincide with the physical

$T$	$N_s^3 \times N_\tau$	$n^{\frac{1}{4}}$ [MeV]	$4\omega$	$\bar{\rho}$ [fm]	$\bar{\rho}/a$	$\#$	$\cos(2\pi\omega)$	$\langle \ell \rangle$	$\gamma$
$0.80 T_C$	$32^3 \times 10$	198	1.00	0.37	2.66	777	0.00	$0.13 \pm 0.01$	$1.61 \pm 0.01$
$0.90 T_C$	$32^3 \times 9$	198	1.00	0.37	2.69	591	0.00	$0.14 \pm 0.01$	$1.65 \pm 0.01$
$1.00 T_C$	$32^3 \times 8$	198	1.00	0.37	2.67	526	0.00	$0.14 \pm 0.01$	$1.69 \pm 0.01$
$1.10 T_C$	$32^3 \times 8$	178	0.61	0.33	2.62	160	0.58	$0.43 \pm 0.01$	$1.29 \pm 0.01$
$1.20 T_C$	$32^3 \times 8$	174	0.51	0.31	2.69	160	0.70	$0.59 \pm 0.01$	$1.18 \pm 0.01$
$1.32 T_C$	$32^3 \times 8$	165	0.43	0.28	2.66	160	0.78	$0.72 \pm 0.01$	$1.10 \pm 0.01$

TABLE IV: For the selected temperatures  $T/T_C = 0.8, 0.9, 1.0, 1.10, 1.20, 1.32$  the corresponding model parameters  $n(T)$ ,  $\omega(T)$ ,  $\bar{\rho}(T)$ , chosen according to Section V, as well as the number of configurations  $\#$ , the lattice sizes  $N_s \times N_\tau$ , and the average caloron size in lattice units  $\bar{\rho}/a$  are listed. Furthermore, the measured Polyakov loop  $\langle|\ell|\rangle$  together with the input value  $\cos(2\pi\omega)$  and the action surplus factor  $\gamma$  as defined in (18) are shown.

quark antiquark potential at sufficiently low temperatures due to the effective isotropy of space-time at  $T=0$ . For higher temperatures, spatial Wilson loops do not provide a physical potential. This is obvious, since the spatial string tension stays approximately constant in the confined phase and even rises beyond the critical temperature.

First of all, we check whether the spatial Wilson loops fulfill the area law

$$\langle W(C_{R,R_2}) \rangle \propto e^{-\sigma \cdot R \cdot R_2}. \quad (41)$$

We show in Fig. 8 the negative logarithm of the Wilson loops  $\langle W(C_{R,R_2}) \rangle$  as a function of

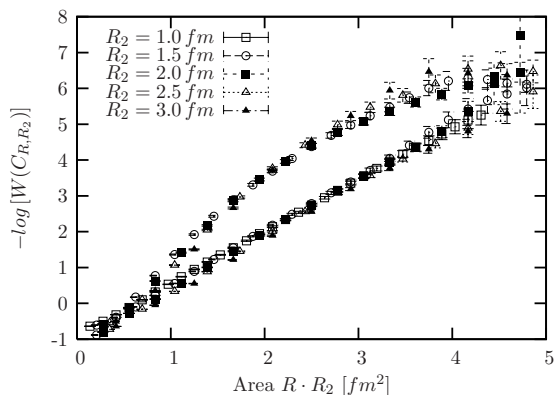


FIG. 8: Negative logarithm of rectangular Wilson loops,  $-\log(W(C_{R,R_2}))$ , with side lengths  $R$ ,  $R_2$  in fundamental (lower curve) and adjoint representation versus the area  $R \cdot R_2$ . The different symbols correspond to different side lengths  $R_2$ .

the enclosed area  $R \cdot R_2$  of the loops. For the fundamental representation (lower curve) the dependence is almost linear as expected, except for some loops with strongly deformed geometry, *i.e.*  $R_2 \gg R$ . This deviation is due to non-area terms

additionally which have been omitted in the exponent of (41). For the adjoint representation,

however, the curve also starts rising linearly at small distances but flattens off at larger  $R$ . This can be seen as a first evidence that screening effects for the adjoint charges can be reproduced by our model.

There are various sources for non-area terms to appear in the exponent of Eq. (41). In general, the effect of various obscuring non-area terms can be compensated by extracting the string tension from certain products of loops of similar shape. A perimeter term, for example, is caused by the self-energy contribution, which is proportional to the perimeter  $R+R_2$ , leading to  $\langle W(C_{R,R_2}) \rangle \propto \exp(-\sigma R R_2 - \alpha(R+R_2) - \gamma)$ . The constant and perimeter terms can be eliminated by calculating the effective string tension from the Creutz ratios [70]

$$\sigma(R, R_2) = \frac{1}{2a^2} \times \ln \left[ \frac{\langle W(C_{R+1, R_2-1}) \rangle \langle W(C_{R-1, R_2+1}) \rangle}{\langle W(C_{R, R_2}) \rangle^2} \right]. \quad (42)$$

However, while the extent  $R_2$  of the contour  $C_{R,R_2}$  should be sufficiently large to suppress contributions of excited states, the expectation value of the Wilson loop increasingly suffers from statistical fluctuations with growing  $R_2$ . Hence, a reasonable value for the side length  $R_2$  has to be chosen to evaluate the effective string tension. As a compromise between systematical and statistical errors we choose the side length  $R_2$  twice as long as  $R$ , *i.e.*  $R_2 = 2 \cdot R$ , which is widely seen as a valid, albeit minimal, condition.

The resulting effective string tensions obtained from Creutz ratios with  $R_2 = 2 \cdot R$  are presented in Fig. 9a for the fundamental representation. For all temperatures shown below  $T_C$  they run into a plateau of approximately  $296 - 318$  MeV/fm within the error bars at moderate distances of about  $R \approx 0.8$  fm. For fixed  $\bar{\rho}(T)$  the observed space-like string tension does only depend weakly on temperature. An ex-



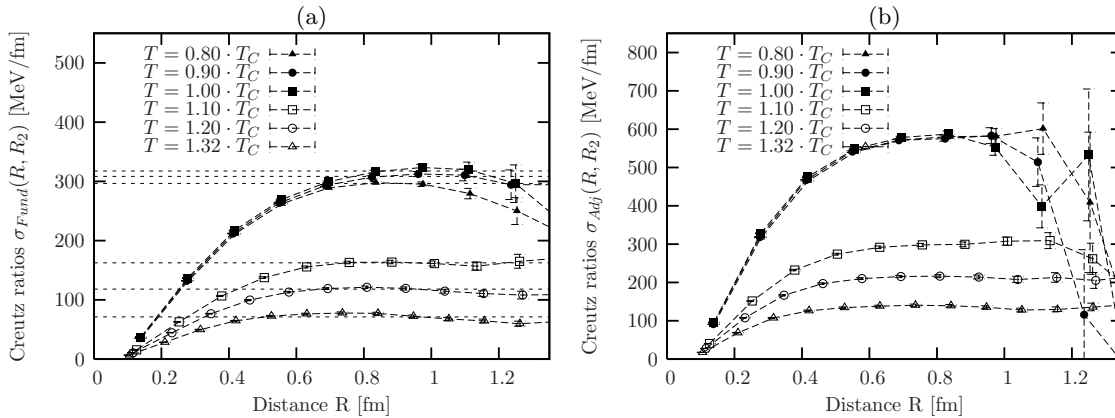


FIG. 9: Effective string tension  $\sigma(R, R_2)$  calculated by Creutz ratios (with  $R_2=2 \cdot R$ ) from spatial Wilson loops versus the distance  $R$  at different temperatures  $T/T_C=0.8, 0.9, 1.0$  for the confined and at  $T/T_C=1.10, 1.20, 1.32$  for the deconfined phase in the fundamental (a) and in the adjoint (b) representation.

act temperature independence could easily be obtained by a minimal change of the average caloron size due to its strong effect on the space-like string tension. For the presented temperatures corresponding to the deconfined phase the spatial string tension runs into plateaux at somewhat smaller distances. The corresponding values of the string tension are strongly reduced compared to the confined phase. This is due to the decreased caloron density, which was chosen according to the drop of the topological susceptibility  $\chi(T)$  in the deconfined phase. This is a limitation of the current model focussing on (anti-)self-dual monopoles as the exclusive origin of the spatial string tension.

All curves, however, tend to fall off as  $R$  increases. If one takes this noisy observation serious it would be interesting to study the contribution of caloron systems to very large Wilson loops analytically. Since the caloron gauge fields become Abelian far outside their cores, it is even worthwhile and instructive to consider only the contributions of the (Abelian) caloron far fields of a caloron gas to very large Wilson loops. Such analytical calculations are currently under consideration [71].

Fig. 9b shows the effective adjoint string tensions, which are expected to run into plateaux before falling off due to adjoint charges being screened by gluons. In our model, in the confined phase the adjoint string tensions reach plateaux of 580 MeV/fm at a distance of  $R \approx 0.8$  fm. At larger distances the color screening sets in, forcing the adjoint force to fall off. We could clearly observe the takeover by screening effects in the confined phase at distances  $R \approx 1$  fm

when considering “square” Creutz ratios with  $R_2=R$ . However, for the extended Creutz ratios with  $R_2=2R$  the signal becomes very noisy at  $R > 1$  fm, and hence, we can only see slight indications for screening effects here. For the deconfined phase the adjoint forces are much smaller than below the critical temperature, due to the reduced caloron density.

Finally, the Casimir scaling hypothesis can be checked. While the scaling of the forces (according to the quadratic Casimir operators) between sources in various representations of the color group is primarily a property of the one-gluon exchange, it holds surprisingly well also at intermediate distances, thus constraining the confining mechanisms. It was an argument against the instanton forces that the Casimir scaling would be strongly violated [72]. The ratio  $\sigma^{adj}(R)/\sigma^{fund}(R)$  obtained in our model is plotted versus the quark separation  $R$  in Fig. 10. It can be seen that the ratio of adjoint and fundamental effective string tensions begins very close to the predicted value at small distances.

## B. Polyakov loops

With the parameters of the model fixed, we are turning now again to the question of confinement at finite temperature based on the Polyakov loop. The color averaged free energy  $F^{avg}(R)$  is derived from the Polyakov loop correlator by Eq. (20) and is presented in Fig. 11a. For the temperatures belonging to the confined phase the short distance behavior of the free energy is independent of the temperature. This has also been ob-

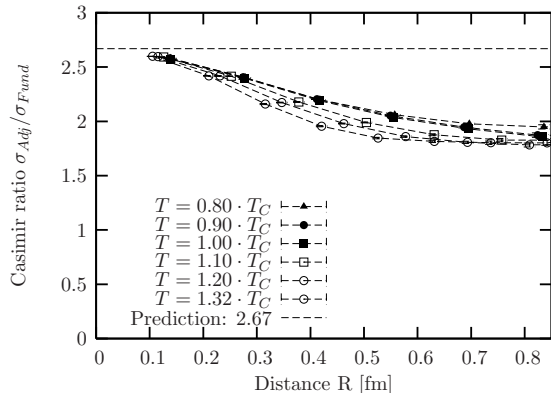


FIG. 10: Casimir ratio  $\sigma_{Adj}/\sigma_{Fund}$  of adjoint and fundamental forces from space-like Wilson loops versus the distance  $R$  at the different temperatures  $T/T_C=0.8, 0.9, 1.0$  for the confined phase and at  $T/T_C=1.10, 1.20, 1.32$  for the deconfined phase. The theoretical prediction of Casimir scaling is marked by the horizontal dashed line.

served in lattice studies [48]. At larger distances the curves become linear and dependent on temperature. What one would expect for the quark-antiquark free energy in the confined phase is a linear behavior at large distances.

This is a consequence of a flux tube forming between the sources. The flux tube is sometimes understood as an elastic string. Due to higher string excitations of the color flux tube, one would expect corrections to this linear behavior. It remains to be seen whether the caloron gas model can generate such a behavior besides the linear confinement corresponding to a stiff flux tube.

The next-to-leading order correction is a  $-\gamma_L/r$  term, the so-called Lüscher term [73]. Its coefficient is universally given by  $\gamma_L=(d-2)\pi/24$ , where  $d$  denotes the space-time dimension. This correction is valid for a large class of effective bosonic string theories at sufficiently large distances. We therefore consider the expression

$$F^{avg}(R, T) = -\frac{A(T)}{R} + \sigma(T) \cdot R + C(T) \quad (43)$$

with the free parameters  $A(T)$ ,  $\sigma(T)$ ,  $C(T)$  as the appropriate fitting function for the measured free energies in the confined phase at not too small distances. Our model is based on long-ranged gauge field excitations, and is therefore not meant to describe short-ranged physics. As a rough estimation we assume the model to become valid at distances larger than the average caloron diameter, *i.e.* for  $R > 2\bar{\rho}(T)$ . We there-

fore fit the quark-antiquark free energy  $F^{avg}(R)$  to Eq. (43) only for these distances, as shown in Fig. 11a. One sees that the measured free energy agrees very well with the expected behavior.

The string tensions obtained from these fits are listed in Table V together with lattice results [48] for the quark-antiquark free energy obtained for  $SU(2)$ . The comparison with the lattice study shows on one hand that our results for the quark-antiquark free energy are of the right order of magnitude (at least for  $T/T_C=0.8, 0.9$ ), but on the other hand it also reveals that our model is, in its present usage, not capable of reproducing the vanishing of the time-like string tension at  $T \rightarrow T_C$ . A possible cure for this limitation of the model will be discussed in the conclusions.

The corresponding coefficients  $A(T)$  belonging to the  $1/r$  correction term are shown in Table V and should be compared with the Lüscher coefficient [73]  $\gamma_L=(d-2)\pi/24 = 0.26$ . It can be seen that the observations are in qualitative agreement with the size of the Lüscher term.

While the quark-antiquark free energy rises linearly at large distances for the confined phase, the picture changes completely beyond the phase transition. Here, the potentials run into plateaux providing zero string tension at large distances. This effect is due to the holonomy deviating from its maximally non-trivial setting. In Section IV we have already seen that the holonomy parameter alone is sufficient to determine whether a caloron ensemble provides a confining potential or not. The decreasing caloron density certainly influences the strength of the obtained potential but is not responsible for the plateau building as such. For increasing temperatures the holonomy parameter becomes closer to trivial and therefore the plateau building already sets in at smaller distances.

For the deconfined phase we have again fitted the measured potential with (43) just to check the vanishing of the time-like string tension. Indeed, almost vanishing string tensions have been obtained. Additionally, we have also tried to fit the model potentials with some exponentially screened expression, since one sees such Yukawa-like behavior in Monte-Carlo simulations [48], but these attempts were unsuccessful.

Additionally, the adjoint charge-anticharge free energy has been determined and is shown in Fig. 11b. Again, the presented potentials coincide at short distances in the confined phase and rise approximately linearly up to distances  $R \approx 1$  fm. At larger distances, the potentials run into plateaux due to string breaking as expected. In the deconfined phase screening effects

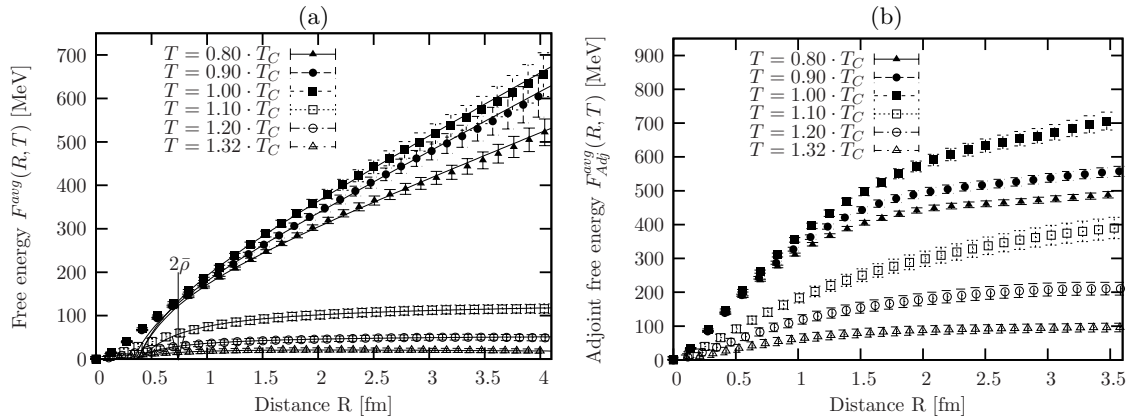


FIG. 11: color averaged free energy versus distance  $R$  at different temperatures  $T/T_C=0.8, 0.9, 1.0$  for the confined and at  $T/T_C=1.10, 1.20, 1.32$  for the deconfined phase in the fundamental (a) and in the adjoint (b) representation. The fundamental potentials are deconfined to (43) for  $R \geq 2\bar{\rho}$ . This minimal distance is marked.

T	$\sigma(T)$ [ $\frac{\text{MeV}}{\text{fm}}$ ]	$\frac{\sigma(T)}{\sigma(0)}$	$\frac{\sigma(T)}{\sigma(0)}$ [48]	$A(T)$
$0.8 T_C$	$100.2 \pm 2.2$	0.31	0.44	$0.33 \pm 0.02$
$0.9 T_C$	$134.1 \pm 1.5$	0.42	0.29	$0.23 \pm 0.02$
$1.0 T_C$	$139.8 \pm 2.1$	0.44	0.00	$0.32 \pm 0.02$

TABLE V: Below  $T_C$ : the string tensions  $\sigma(T)$  and the  $1/r$  fit parameters  $A(T)$  as obtained from fitting the quark-antiquark free energy to (43).  $\sigma(T)$  is presented in physical units and in units of  $\sigma(0)$ , where  $\sigma(0) = 318$  MeV/fm for our model according to Section VC3. For comparison, lattice results for  $\sigma(T)/\sigma(0)$  taken from Ref. [48] are presented.

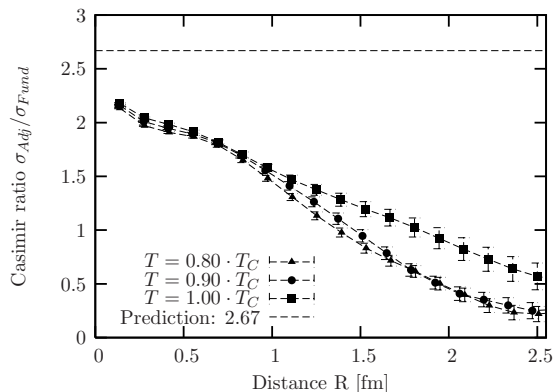


FIG. 12: Ratio  $\sigma_{Adj}/\sigma_{Fund}$  of adjoint and fundamental forces from Polyakov loop correlators versus the distance  $R$  at different temperatures  $T/T_C=0.8, 0.9, 1.0$  for the confined phase. The theoretical prediction of Casimir scaling is marked by the horizontal dashed line.

are also observed.

Finally, the Casimir scaling hypothesis shall be checked. We show the Casimir ratio  $\sigma^{adj}(R)/\sigma^{fund}(R)$  together with its prediction at short distances in Fig. 12. It can be seen that the

measured ratio reproduces approximately 85 % of the theoretical prediction. Here, the deviation from Casimir scaling is much stronger than in the previously discussed case of the space-like string tension.

## VII. MAGNETIC MONOPOLE CURRENTS

In the dual superconductor picture of confinement proposed by 't Hooft [74] and Mandelstam [75], the observation of a linearly rising quark-antiquark potential is explained by the formation of narrow flux tubes of the chromoelectric field. Once such field is inserted to the vacuum by quark sources it is squeezed under the influence of a vacuum “pressure” provided by a Higgs condensate. Furthermore, 't Hooft also conjectured that the relevant degrees of freedom responsible for the confinement property of this theory are actually  $U(1)$  degrees of freedom. Therefore, one expects the QCD vacuum in the confined phase to be populated by random world lines of Abelian magnetic monopoles (Dirac monopoles), the origin of the Higgs condensate. If there are electric

flux tubes, they are enclosed by additional coherent azimuthal magnetic eddy currents. The necessary condition for the viability of this description is the possibility of percolation of Abelian magnetic currents. It is therefore of interest whether, in the KvBLL caloron gas model, percolation of Abelian magnetic currents can be observed.

The Abelian magnetic currents should be observable after fixing an Abelian gauge and splitting the gauge field into a (dominating at large distances) Abelian component and (important only at short distances) non-Abelian components.

The maximally Abelian gauge (MAG) is the most suitable gauge for the purpose of this decomposition. In this gauge, even the neglect of the non-Abelian degrees of freedom is a reasonable approximation. The maximally Abelian gauge (MAG) is defined as the gauge maximizing the gauge functional

$$R = \sum_{x,\mu} Tr [\tau_3 U_{x,\mu} \tau_3 U_{x,\mu}^\dagger] \quad (44)$$

by exploiting the non-Abelian gauge freedom. Once the extremization is achieved, on average all link variables  $U_{x,\mu}$  are as close as possible to links  $U'_{x,\mu}$  belonging to the Abelian subgroup  $\{\exp(i\phi\tau_3) : \phi \in [0 : 2\pi]\} \subset SU(2)$ . The projection

$$U_{x,\mu} = u_0 + i\vec{u}\vec{\tau} \rightarrow U'_{x,\mu} = \exp(i\theta_{x,\mu}\tau_3) \quad (45)$$

from  $SU(2)$  to  $U(1)$  is tantamount to suppressing  $u_1$  and  $u_2$ , keeping only the phase  $\theta_{x,\mu} = \arg(u_0 + iu_3)$  as the  $U(1)$  gauge field. The  $U(1)$  gauge freedom of the remaining Abelian gauge field  $\theta_{x,\mu}$  remains unfixed. The Abelian monopole currents  $j_\mu^{mag}$  can be associated with the Abelian projected gauge field in the same way as in compact QED [76].

Due to magnetic charge conservation  $\partial_\mu j_\mu^{mag} = 0$ , the magnetic currents build closed loops (clusters) on a finite and periodic lattice. In Monte Carlo simulations on sufficiently large lattices the network of monopole clusters was found to be composed of a single very large cluster traversing the whole volume and many other clusters of small size. The histogram  $h(l)$  representing the abundance of connected clusters containing monopole world lines of total length  $l$  (defined by counting the occupied links) was found to be split into two very distinctive parts,  $h_{UV}(l)$  for the small clusters and  $h_{IR}(l)$  for the percolating ones, with a gap separating the two [77, 78]. The percolating cluster alone was shown to reproduce almost the full monopole

string tension, meaning that the remaining small clusters are not relevant for confinement. Furthermore, the 3-dimensional (dimensionful) density  $n_{IR}^{(3D)}$  of magnetic currents belonging to the percolating cluster has been found to be related to the string tension by  $n_{IR}^{(3D)}/\sigma^{3/2} = 0.65(2)$  for MAG [79]. Although the exact ratio depends on the chosen Abelian gauge fixing procedure (and is not universal for all possible non-Abelian actions) [80], the percolation itself of magnetic currents, more precisely non-vanishing winding in spatial directions, is an indication for quark confinement.

Fig. 13 shows the average numbers of clusters of a certain size per configuration as histograms of monopole clusters with respect to their length (participating links) in lattice units,  $h(l)$ , and with respect to their maximal 3-dimensional extension,  $H(R^{(3D)})$ . The histograms have been evaluated for 160 configurations for each of the temperatures  $T/T_C = 0.8, 0.9, 1.0$  in the confined phase. These measurements have been made on *periodic* lattices, in contrast to the open volume simulations described above. Since calorons are *not* periodic regarding the *space-like* dimensions, special care has to be taken to minimize the resulting action surplus created by bringing the caloron ensemble onto a periodic lattice. We therefore compute for every space-time position  $x$  the analytic, single caloron vector potential  $A_\mu^{(i)}(\Delta x \equiv x^{(i)} - x)$ , where  $x^{(i)}$  is the position of the  $i$ -th caloron, guaranteeing by appropriate shift operations that the inevitable discontinuity of each caloron's vector potential appears at only those space-time positions (on the antipodal side of the torus) where the gauge fields are minimal, thus minimizing the action surplus. Except for this difference, all model parameters corresponding to these selected temperatures are chosen according to Table IV as before.

Due to the periodicity a subtle definition of the cluster extension  $R^{(3D)}$  is needed. At first, the smallest cuboid circumscribing the cluster is determined. If the extent of this cuboid is smaller than the lattice size in all directions, then the distance between all cluster points is unambiguously defined. In the opposite case, the cluster can be considered as percolating (in one or more directions). The observed cluster sizes are much larger than the average caloron size  $\bar{\rho} = 0.37$  fm. A small fraction of the clusters percolate in the sense defined above, and some of these clusters wrap around the periodic lattice in the space-like directions, carrying a non-zero winding number. As discussed above this is a signal for confinement.

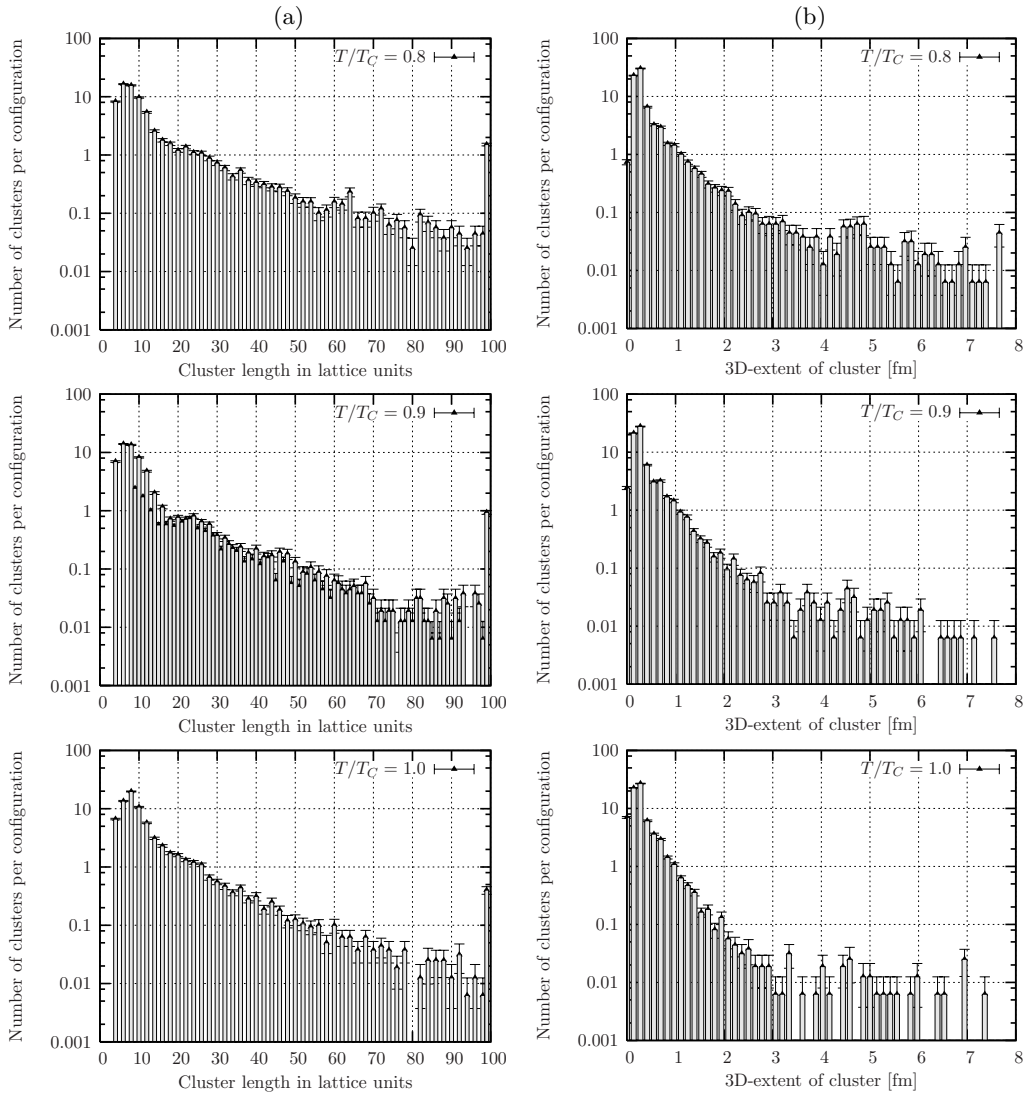


FIG. 13: Histograms showing the average number of clusters per configuration of a certain cluster size, in (a) characterized by the number of occupied links in the cluster, in (b) characterized by the 3D extent of the cluster, for the temperatures  $T/T_C = 0.8, 0.9, 1.0$  in the confined phase. Link numbers larger than 100 are set equal to 100.

In contrast to that, the pictures look completely different for temperatures above  $T_c$ . Fig. 14 shows the histograms of monopole clusters with respect to their length in lattice units,  $h(l)$ , and with respect to their maximal 3-dimensional extension,  $H(R^{(3D)})$ . Again, 160 configurations have been evaluated for each of the temperatures  $T/T_C = 1.10, 1.20, 1.32$  in the deconfined phase. One sees that both distributions are strongly contracted towards smaller cluster sizes. No percolation or wrapping around the lattice is encountered anymore for temperatures above the critical temperature. This observation is in agreement with the breakdown of (time-like)

confinement that we had found from the study of the Polyakov correlators.

However, it should be noted that the actual sizes  $l$  of the percolating clusters are one or two orders of magnitude smaller than those seen in the Monte Carlo ensembles [80]. This is only natural since the presently evaluated configurations are constructed by superposing single calorons. Each non-dissociated caloron gives rise to a closed cluster traversing through both of its constituents such that this cluster entirely lies within the caloron core. For dissociated calorons two disconnected monopole clusters (world lines) emerge wrapping around the periodic lattice in

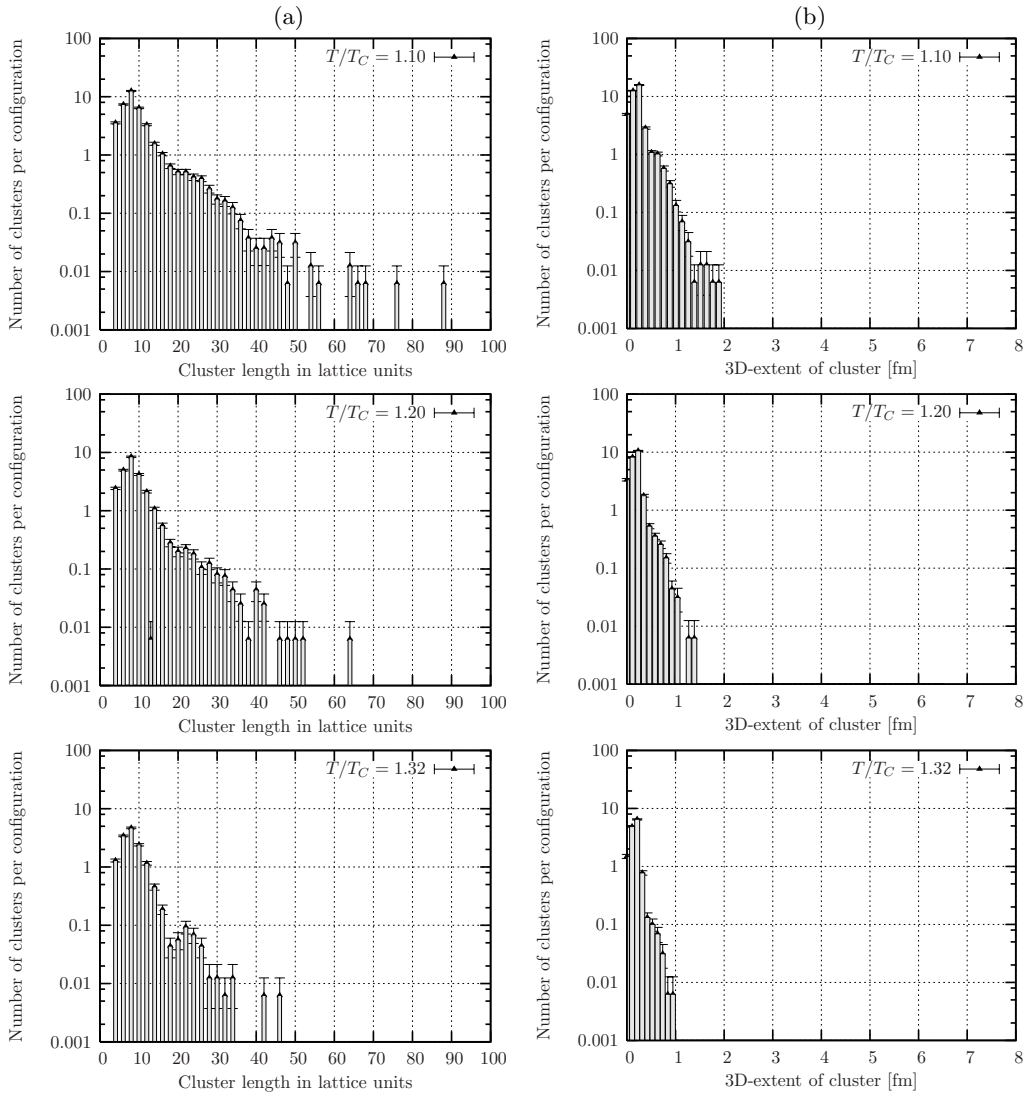


FIG. 14: Histograms showing the average number of clusters per configuration of a certain cluster size, in (a) characterized by the number of occupied links in the cluster, in (b) characterized by the 3D extent of the cluster, for the temperatures  $T/T_C = 1.10, 1.20, 1.32$  in the deconfined phase.

time direction. Since the caloron gauge field is non-Abelian only in its core, and the vector potential away from the core can be approximately identified by the Abelian projection, the resulting multi-caloron gauge field is Abelian almost everywhere. Since the calorons are sitting relatively close, the monopole world lines reorganize themselves into a percolating network without essentially increasing the density of monopole currents. Hence, the observed monopole cluster sizes in the confinement phase are barely exceeding the minimal cluster sizes necessary to facilitate the required monopole percolation. This can be seen, if one compares the average monopole cluster length in lattice units, as measured in

the simulation, with the average cluster length, that would be obtained, if each single caloron's monopole cluster was not effected by the presence of the other calorons. Table VI shows simulation results together with the estimates for the average cluster length, as obtained from the given  $\rho$ -distribution with  $\bar{\rho} = 0.37$  fm. It can be seen that the total length of the monopole clusters induced by the single calorons is increased only by 25 – 35% in order to unite closely situated monopole clusters to form a connected monopole cluster.

$T$	Measured	Estimated
$0.8 T_C$	14.7	11.5
$0.9 T_C$	14.1	10.9
$1.0 T_C$	12.4	9.2

TABLE VI: Average cluster lengths in lattice units as measured in the simulations. The result is compared to an estimate given by the caloron  $\rho$  distribution, assuming each single caloron monopole cluster to be unaltered by the presence of other calorons.

### VIII. SUMMARY AND CONCLUSIONS

We have introduced a semi-classical model meant to describe the Euclidean field histories of (quenched) QCD as a dilute gas of KvBLL calorons with adjustable holonomy. We have shown, that this has the striking impact that the confinement/deconfinement phase transition can in principle be modelled by varying nothing but the holonomy parameter, starting from its maximally non-trivial value  $\omega(T < T_C) = 0.25$  for the confined phase, towards its trivial setting  $\omega(T \gg T_C) \rightarrow 0$  or  $0.5$ , respectively, as the temperature increases, such that very high above the critical temperature the well-known HS-caloron is finally recovered.

In order to work out the model more quantitatively and in detail, the parameters of this model have been chosen in agreement with lattice observations. Firstly, the holonomy parameter  $\omega(T)$  was fixed in accordance with lattice studies of the renormalized Polyakov loop in  $SU(2)$  by exploiting the low-density relation  $\langle |\ell| \rangle = \cos(2\pi|\vec{\omega}|)$ . The reliability of the current determination of  $\omega(T)$  could be improved, if it would be determined in a self-consistent manner. However, as long as the holonomy is maximally non-trivial in the confined phase and becomes trivial only at high temperatures above  $T_C$ , the exact functional form of  $\omega(T)$  has only little influence on the observed “asymptotic” string tensions.

Second, the caloron density  $n(T)$  has been determined by lattice results for the topological susceptibility  $\chi(T)$  by assuming calorons and anticalorons to be uncorrelated. Since we do not take any caloron/anticaloron correlation into account for the sampling of their positions, this is the adequate assumption with respect to our model, although calorons and anticalorons are actually known to be correlated. This has lead us to adopt a constant caloron density  $n(T) = 1 \text{ fm}^{-4}$  as usual in the confined phase and a decreasing density  $\propto \chi(T)$  in the deconfined phase. This is not compelling since the

decreasing topological susceptibility could also be explained by topologically uncharged objects becoming dominant, such as caloron-anticaloron molecules, although there is no independent indication for that to happen in quenched QCD.

Also in another respect the current model is incomplete in the deconfined phase because it does not consider non-perturbative configurations of other origin. This incompleteness becomes obvious by seeing the space-like string tension decreasing above the critical temperature due to the reduced caloron density. This is unphysical since the space-like string tension is known to rise at higher temperatures, completely independent from the topological susceptibility which becomes tiny. Apart from the loophole forcing us to accept a decreasing density of calorons, it could well be that monopoles being neither self-dual nor anti-self-dual build the spatial string tension throughout the deconfined phase.

The breakdown of the physically confining potentials above the critical temperature in our model is driven by the holonomy alone. The decrease of the caloron density would not be required.

Third, the  $\rho$ -distribution was determined by reinterpreting the single caloron quantum weight in the dense-packing limit. Due to its divergence at  $\rho \rightarrow \infty$  for non-trivial holonomy, additional arguments rendering the  $\rho$ -distribution finite had to be invoked. Since its analytical form could only be qualitatively motivated, a more sound investigation of the  $\rho$ -distribution in a dense medium of calorons would be worthwhile. However, having fixed the analytical form of the size distribution, the average caloron size in the confined phase has been unambiguously determined by comparing the space-like string tensions with those obtained in lattice studies. Hence, the usual criticism of instanton/caloron based models, namely that almost every desired result could be obtained from this kind of models by suitably setting the average caloron size, is actually not applicable here.

The color-averaged quark-antiquark free energy was then extracted from the Polyakov loop correlation in multi-caloron configurations constructed according to a simple superposition scheme. Since our model is based on long-ranged gauge field excitations of average diameter  $2\bar{\rho}(T)$ , the model is not supposed to yield reasonable results at distances smaller than  $R < 2\bar{\rho}(T)$ . For  $R > 2\bar{\rho}(T)$  the obtained free energies show the expected linear plus Lüscher term behavior up to distances of  $R \approx 4 \text{ fm}$  in the confined phase. Above the critical temperature the obtained po-

tentials run into plateaux corresponding to the deconfinement of quarks. The obtained string tensions are of the correct order of magnitude as can be seen by a comparison with lattice studies. However, our model is, so far, not capable to reproduce the correct temperature dependence of the time-like (color-averaged) string tension, which is known to gradually decrease with rising temperature before it is going to vanish at  $T = T_C$ . This limitation is caused by the fact that our model does not allow for mixed holonomies within a single gauge field configuration. A minimal improvement of the model would be to sample the uniform caloron holonomies in the confined phase according to a distribution with non-vanishing, temperature dependent width (in accordance to what is seen in lattice Monte Carlo simulations) rather than being fixed exactly to zero ( $\omega = 0.25$ ).

By studying the potentials in the adjoint representation screening effects due to string breaking could be observed. For small distances a ratio between the fundamental and adjoint effective string tensions of  $\sigma^{adj}/\sigma^{fund} \approx 2.2$  was obtained, which is close to but smaller than the ratio  $8/3$  predicted by the Casimir scaling hypothesis. For space-like string tensions screening effects could also be seen and the Casimir hypothesis was even better fulfilled. Here, a ratio  $\sigma^{adj}/\sigma^{fund} \approx 2.6$  could be observed for all selected confining temperatures.

Finally, the formation of large magnetic monopole clusters was studied in the caloron gas model. Percolating clusters traversing the whole lattice volume were observed for the confining phase, which is a necessary condition for confinement. For the deconfined phase the distribution of monopole cluster sizes is contracted towards smaller cluster sizes and no spatially perm-

colating clusters are found anymore, which is in agreement with Monte Carlo lattice observations. Not unexpectedly, the observed monopole clusters are one or two orders of magnitude smaller (in path length) than those obtained in Monte Carlo studies. The average cluster lengths in the caloron ensembles are only slightly increased by rearrangements induced by the caloron superposition compared to the sum of the cluster sizes of the separate calorons.

In conclusion we would like to say, despite the limitations that our model still suffers from, the KvBLL caloron gas model offers an interesting scenario for the confinement/deconfinement phase transition. With the proposed improvements, the KvBLL caloron gas model most probably will give a consistent picture of the phase transition. Therefore it is a worthwhile topic to further investigation.

#### Acknowledgements

We would like to thank Boris Martemyanov for introducing the idea how to superpose KvBLL calorons with non-trivial holonomy. We are grateful to Falk Bruckmann for sharing his insights on KvBLL caloron systems and for enlightening discussions and correspondence. We appreciate the support from Pierre van Baal, having organized a meeting in Leiden one year ago, and his recent helpful comments on this paper prior to publication. We thank Olaf Kaczmarek for drawing our attention to Ref. [48] and the authors of this work for the kind permission to use their results in Fig. 4. Finally, we are grateful to Alexander Veselov for providing the code for MAG fixing based on the simulated annealing algorithm.

- 
- [1] C. G. Callan (Jr), R. F. Dashen, and D. J. Gross. *Phys. Rev.*, D17:2717, 1978.
  - [2] A. A. Belavin, A. M. Polyakov, A. S. Shvarts, and Y. S. Tyupkin. *Phys. Lett.*, B59:85–87, 1975.
  - [3] E. V. Shuryak. *Nucl. Phys.*, B198:83, 1982.
  - [4] E. V. Shuryak and J. J. M. Verbaarschot. *Phys. Rev.*, D52:295–306, 1995.
  - [5] T. Schäfer and E. V. Shuryak. *Phys. Rev.*, D53:6522–6542, 1996.
  - [6] J. W. Negele, F. Lenz, and M. Thies. *Nucl. Phys. Proc. Suppl.*, 140:629–631, 2005.
  - [7] J.-L. Gervais and B. Sakita. *Phys. Rev.*, D11:2943, 1975.
  - [8] E.-M. Ilgenfritz, M. L. Laursen, G. Schierholz, M. Müller-Preussker, and H. Schiller. *Nucl. Phys.*, B268:693, 1986.
  - [9] M. Teper. *Phys. Lett.*, B171:86, 1986.
  - [10] J. Hoek, M. Teper, and J. Waterhouse. *Nucl. Phys.*, B288:589, 1987.
  - [11] M. I. Polikarpov and A. I. Veselov. *Nucl. Phys.*, B297:34, 1988.
  - [12] M. C. Chu, J. M. Grandy, S. Huang, and J. W. Negele. *Phys. Rev.*, D49:6039–6050, 1994.
  - [13] T. A. DeGrand, A. Hasenfratz, and T. G. Kovacs. *Nucl. Phys.*, B520:301–322, 1998.
  - [14] G. 't Hooft. *Phys. Rev.*, D14:3432–3450, 1976.
  - [15] E.-M. Ilgenfritz and M. Müller-Preussker. *Nucl. Phys.*, B184:443, 1981.
  - [16] D. Diakonov and V. Y. Petrov. *Nucl. Phys.*, B245:259, 1984.



- [17] T. Banks and A. Casher. *Nucl. Phys.*, B169:103, 1980.
- [18] E. V. Shuryak and J. J. M. Verbaarschot. *Nucl. Phys.*, B410:55–89, 1993.
- [19] T. Schäfer, E. V. Shuryak, and J. J. M. Verbaarschot. *Nucl. Phys.*, B412:143–168, 1994.
- [20] T. Schäfer and E. V. Shuryak. *Phys. Rev.*, D50:478–485, 1994.
- [21] G. 't Hooft. *Phys. Rev. Lett.*, 37:8–11, 1976.
- [22] D. Chen, R. C. Brower, J. W. Negele, and E. V. Shuryak. *Nucl. Phys. Proc. Suppl.*, 73:512–514, 1999.
- [23] T. C. Kraan and P. van Baal. *Phys. Lett.*, B428:268–276, 1998.
- [24] T. C. Kraan and P. van Baal. *Nucl. Phys.*, B533:627–659, 1998.
- [25] T. C. Kraan and P. van Baal. *Phys. Lett.*, B435:389–395, 1998.
- [26] K.-M. Lee and C.-H. Lu. *Phys. Rev.*, D58:025011, 1998.
- [27] D. Diakonov, N. Gromov, V. Petrov, and S. Slizovskiy. *Phys. Rev.*, D70:036003, 2004.
- [28] E.-M. Ilgenfritz, B. V. Martemyanov, M. Müller-Preussker, S. Shcheredin, and A. I. Veselov. *Phys. Rev.*, D66:074503, 2002.
- [29] F. Bruckmann, E. M. Ilgenfritz, B. V. Martemyanov, and P. van Baal. *Phys. Rev.*, D70:105013, 2004.
- [30] E.-M. Ilgenfritz, B. V. Martemyanov, M. Müller-Preussker, and A. I. Veselov. *Phys. Rev.*, D73:094509, 2006.
- [31] E.-M. Ilgenfritz, B. V. Martemyanov, M. Müller-Preussker, and A. I. Veselov. *Phys. Rev.*, D71:034505, 2005.
- [32] C. Gattringer. *Phys. Rev.*, D67:034507, 2003.
- [33] C. Gattringer and S. Schaefer. *Nucl. Phys.*, B654:30–60, 2003.
- [34] C. Gattringer, E.-M. Ilgenfritz, B. V. Martemyanov, M. Müller-Preussker, D. Peschka, R. Pullirsch, S. Schaefer, and A. Schäfer. *Nucl. Phys. Proc. Suppl.*, 129:653–658, 2004.
- [35] F. Bruckmann, E.-M. Ilgenfritz, B. V. Martemyanov, M. Müller-Preussker, D. Negradi, D. Peschka, and P. van Baal. *Nucl. Phys. Proc. Suppl.*, 140:635–646, 2005.
- [36] E. M. Ilgenfritz, M. Müller-Preussker, and D. Peschka. *Phys. Rev.*, D71:116003, 2005.
- [37] M. F. Atiyah, N. J. Hitchin, V. G. Drinfeld, and Y. I. Manin. *Phys. Lett.*, A65:185–187, 1978.
- [38] B. J. Harrington and H. K. Shepard. *Phys. Rev.*, D17:2122, 1978.
- [39] D. J. Gross, R. D. Pisarski, and L. G. Yaffe. *Rev. Mod. Phys.*, 53:43, 1981.
- [40] N. Weiss. *Phys. Rev.*, D24:475, 1981.
- [41] M. K. Prasad and C. M. Sommerfield. *Phys. Rev. Lett.*, 35:760–762, 1975.
- [42] F. Bruckmann and P. van Baal. *Nucl. Phys.*, B645:105–133, 2002.
- [43] F. Bruckmann, D. Negradi, and P. van Baal. *Nucl. Phys.*, B698:233–254, 2004.
- [44] E. V. Shuryak. *Phys. Lett.*, B153:162, 1985.
- [45] A. Dumitru, Y. Hatta, J. Lenaghan, K. Orginos, and R. D. Pisarski. *Phys. Rev.*, D70:034511, 2004.
- [46] A. M. Polyakov. *Nucl. Phys.*, B164:171–188, 1980.
- [47] J.-L. Gervais and A. Neveu. *Nucl. Phys.*, B163:189, 1980.
- [48] S. Digal, S. Fortunato, and P. Petreczky. *Phys. Rev.*, D68:034008, 2003.
- [49] O. Kaczmarek, F. Karsch, F. Zantow, and P. Petreczky. *Phys. Rev.*, D70:074505, 2004.
- [50] E. Witten. *Nucl. Phys.*, B156:269, 1979.
- [51] G. Veneziano. *Nucl. Phys.*, B159:213–224, 1979.
- [52] E.-M. Ilgenfritz and M. Müller-Preussker. *Phys. Lett.*, B99:128, 1981.
- [53] C. Gattringer, R. Hoffmann, and S. Schaefer. *Phys. Lett.*, B535:358–362, 2002.
- [54] N. Cundy, M. Teper, and U. Wenger. *Phys. Rev.*, D66:094505, 2002.
- [55] L. Del Debbio, L. Giusti, and C. Pica. *Phys. Rev. Lett.*, 94:032003, 2005.
- [56] P. H. Ginsparg and K. G. Wilson. *Phys. Rev.*, D25:2649, 1982.
- [57] P. Hasenfratz, V. Laliena, and F. Niedermayer. *Phys. Lett.*, B427:125–131, 1998.
- [58] B. Alles, M. D’Elia, and A. Di Giacomo. *Phys. Lett.*, B412:119–124, 1997.
- [59] B. Alles, M. D’Elia, A. Di Giacomo, and R. Kirchner. *Nucl. Phys. Proc. Suppl.*, 63:510–512, 1998.
- [60] E.-M. Ilgenfritz and E. V. Shuryak. *Phys. Lett.*, B325:263–266, 1994.
- [61] E. V. Shuryak. *Phys. Rev.*, D52:5370–5373, 1995.
- [62] N. O. Agasian and Y. A. Simonov. *Mod. Phys. Lett.*, A10:1755–1760, 1995.
- [63] D. Diakonov and V. Petrov. talk given at the International Workshop on Nonperturbative Approaches to QCD, Trento, Italy, 10-29 Jul 1995.
- [64] G. Münster and C. Kamp. *Eur. Phys. J.*, C17:447–454, 2000.
- [65] G. Münster. *Zeit. Phys.*, C12:43, 1982.
- [66] T. C. Kraan. *Commun. Math. Phys.*, 212:503–533, 2000.
- [67] M. C. Chu and S. Schramm. *Phys. Rev.*, D51:4580–4586, 1995.
- [68] R. Hofmann. *Int. J. Mod. Phys.*, A20:4123, 2005.
- [69] B. Lucini, M. Teper, and U. Wenger. *JHEP*, 02:033, 2005.
- [70] M. Creutz. *Phys. Rev.*, D21:2308–2315, 1980.
- [71] F. Bruckmann. Private communication.
- [72] V. I. Shevchenko and Yu. A. Simonov. *Phys. Rev. Lett.*, 85:1811–1814, 2000.
- [73] M. Lüscher, K. Symanzik, and P. Weisz. *Nucl. Phys.*, B173:365, 1980.
- [74] G. 't Hooft. Rapporteur’s talk given at Int. Conf. on High Energy Physics, Palermo, Italy, Jun 23–28, 1975.
- [75] S. Mandelstam. *Phys. Rept.*, 23:245–249, 1976.
- [76] T. A. DeGrand and D. Toussaint. *Phys. Rev.*, D22:2478, 1980.

- [77] A. Hart and M. Teper. *Phys. Rev.*, D58:014504, 1998.
- [78] A. Hart and M. Teper. *Phys. Rev.*, D60:114506, 1999.
- [79] V. Bornyakov and M. Müller-Preussker. *Nucl. Phys. Proc. Suppl.*, 106:646–648, 2002.
- [80] V. G. Bornyakov, E.-M. Ilgenfritz, and M. Müller-Preussker. *Phys. Rev.*, D72:054511, 2005.